

C-type natriuretic peptide facilitates autonomic Ca^{2+} entry in growth plate chondrocytes for stimulating bone growth

Yuu Miyazaki^{1†}, Atsuhiko Ichimura^{1†}, Ryo Kitayama¹, Naoki Okamoto¹, Tomoki Yasue¹, Feng Liu¹, Takaaki Kawabe¹, Hiroki Nagatomo¹, Yohei Ueda², Ichiro Yamauchi², Takuro Hakata², Kazumasa Nakao², Sho Kakizawa¹, Miyuki Nishi¹, Yasuo Mori³, Haruhiko Akiyama⁴, Kazuwa Nakao⁵, Hiroshi Takeshima^{1*}

¹Graduate School of Pharmaceutical Sciences, Kyoto University, Kyoto, Japan; ²Graduate School of Medicine, Kyoto University, Kyoto, Japan; ³Graduate School of Engineering, Kyoto University, Kyoto, Japan; ⁴Graduate School of Medicine, Gifu University, Gifu, Japan; ⁵Medical Innovation Center, Kyoto University, Kyoto, Japan

Abstract The growth plates are cartilage tissues found at both ends of developing bones, and vital proliferation and differentiation of growth plate chondrocytes are primarily responsible for bone growth. C-type natriuretic peptide (CNP) stimulates bone growth by activating natriuretic peptide receptor 2 (NPR2) which is equipped with guanylate cyclase on the cytoplasmic side, but its signaling pathway is unclear in growth plate chondrocytes. We previously reported that transient receptor potential melastatin-like 7 (TRPM7) channels mediate intermissive Ca^{2+} influx in growth plate chondrocytes, leading to activation of Ca^{2+} /calmodulin-dependent protein kinase II (CaMKII) for promoting bone growth. In this report, we provide evidence from experiments using mutant mice, indicating a functional link between CNP and TRPM7 channels. Our pharmacological data suggest that CNP-evoked NPR2 activation elevates cellular cGMP content and stimulates big-conductance Ca^{2+} -dependent K^+ (BK) channels as a substrate for cGMP-dependent protein kinase (PKG). BK channel-induced hyperpolarization likely enhances the driving force of TRPM7-mediated Ca^{2+} entry and seems to accordingly activate CaMKII. Indeed, ex vivo organ culture analysis indicates that CNP-facilitated bone growth is abolished by chondrocyte-specific *Trpm7* gene ablation. The defined CNP signaling pathway, the NPR2-PKG-BK channel-TRPM7 channel-CaMKII axis, likely pinpoints promising target proteins for developing new therapeutic treatments for divergent growth disorders.

***For correspondence:** takeshima.hiroshi.8m@kyoto-u.ac.jp

[†]These authors contributed equally to this work

Competing interest: The authors declare that no competing interests exist.

Funding: See page 20

Received: 05 July 2021

Preprinted: 17 September 2021

Accepted: 27 February 2022

Published: 15 March 2022

Reviewing Editor: Fayeز Safadi, Northeast Ohio Medical University, United States

© Copyright Miyazaki et al. This article is distributed under the terms of the [Creative Commons Attribution License](https://creativecommons.org/licenses/by/4.0/), which permits unrestricted use and redistribution provided that the original author and source are credited.

Editor's evaluation

With the new additional data and descriptions, the paper in its current state is well organized and data presented add a new information on the role of C-type natriuretic peptide and how it facilitates autonomic Ca^{2+} entry in chondrocytes and modulates bone growth.

Introduction

The development of skeletal long bones occurs through endochondral ossification processes, during which chondrocyte layers form the growth plates at both ends of bone rudiments, and then the

expanded cartilage portions are gradually replaced by trabecular bones through the action of osteoclasts and osteoblasts (Berendsen and Olsen, 2015). Therefore, bone size largely depends on the proliferation of growth plate chondrocytes during endochondral development. On the other hand, atrial (ANP), brain (BNP), and C-type (CNP) natriuretic peptides regulate diverse cellular functions by activating the receptor guanylate cyclases, NPR1 and NPR2 (Nakao et al., 1996). Of the natriuretic peptides, CNP exclusively stimulates bone development by acting on growth plate chondrocytes expressing the CNP-specific receptor NPR2 (Nakao et al., 1996; Wit and Camacho-Hübner, 2011; Peake et al., 2014). Indeed, loss- and gain-of-function mutations in the human *NPR2* gene cause acromesomelic dysplasia and skeletal overgrowth disorder, respectively (Vasques et al., 2014; Wit et al., 2016). Furthermore, translational studies have been probing the benefits of CNP treatments in various animal models with impaired skeletal growth, and a phase III clinical trial of CNP therapy has recently been completed and approved for treatment of achondroplasia patients primarily resulting from mutations in the *FGFR3* gene (Savarirayan et al., 2020). It is thus likely that NPR2 guanylate cyclase controls chondrocytic cGMP content during growth plate development. Downstream of NPR2 activation, cGMP-dependent protein kinase (PKG) seems to phosphorylate target proteins to facilitate growth plate chondrogenesis (Peake et al., 2014). Activated PKG is postulated to stimulate the biosynthesis of growth plate extracellular matrix by playing an inhibitory role in the mitogen-activated protein kinase Raf–MEK–ERK cascade (Krejci et al., 2005). In parallel, glycogen synthase kinase 3 β (GSK3 β) is likely activated by PKG-mediated phosphorylation, leading to the hypertrophic maturation of growth plate chondrocytes (Kawasaki et al., 2008). However, it is still unclear how CNP promotes bone growth at the molecular level, and it is important to further address CNP signaling cascade in growth plate chondrocytes.

In the transient receptor potential channel superfamily, the melastatin subfamily member 7 (TRPM7) forms a mono- and divalent cation-permeable channel in various cell types and participates in important cellular processes including cell growth and adhesion (Fleig and Chubanov, 2014). We recently reported that growth plate chondrocytes generate autonomic intracellular Ca²⁺ fluctuations, which are generated by the intermittent gating of TRPM7 channels, and also that TRPM7-mediated Ca²⁺ entry activates Ca²⁺/calmodulin-dependent protein kinase II (CaMKII), facilitating endochondral bone growth (Qian et al., 2019). Based on these observations, we explored the link between CNP signaling and TRPM7-mediated Ca²⁺ entry through the experiments described in this report. Our data obtained clearly indicate that big-conductance Ca²⁺-dependent K⁺ (BK) channels play a key role in the functional coupling between NPR2 and TRPM7 channels in growth plate chondrocytes.

Results

CNP facilitates spontaneous Ca²⁺ fluctuations in growth plate chondrocytes

In the growth plates of developing bones, proliferating cartilage cells, designated as round and columnar chondrocytes, frequently exhibit weak increases and decreases in intracellular Ca²⁺ concentration under resting conditions (Qian et al., 2019). On the other hand, previous *in vivo* studies demonstrated that CNP application (>1 μ mol/kg) stimulates endochondral bone growth (Nakao et al., 1996). In our Fura-2 imaging of round chondrocytes within femoral bone slices prepared from wild-type mice, CNP pretreatments (30–300 nM for 1 hr) dose-dependently facilitated spontaneous Ca²⁺ fluctuations (Figure 1A). In particular, fluctuation-positive cell ratio and fluctuation amplitude were remarkably elevated in response to the CNP treatments. In contrast, ANP treatments exerted no effects on Ca²⁺ fluctuations in growth plate chondrocytes.

In chondrocyte-specific *Npr2*-knockout mice (*Npr2*^{fl/fl}, *Col2a1-Cre*^{+/−}), Cre recombinase is expressed under the control of the collagen type 2 α 1 gene promoter and thus inactivates the floxed *Npr2* alleles in a chondrocyte-specific manner (Nakao et al., 2015). Our RT-PCR analysis indicated that the floxed *Npr2* gene was largely inactivated in the growth plates prepared from the E17.5 mutant embryos, but such recombination events were not detected in other tissues examined (Figure 1—figure supplement 1A, B). Accordingly, *Npr2* mRNA contents in the mutant growth plates were reduced to less than 40% of controls (Figure 1—figure supplement 1C), despite the growth plate preparations contain not only chondrocytes but also perichondrium-resident cells including undifferentiated mesenchymal cells and immature chondroblasts. Further RT-PCR analysis detected similar expression

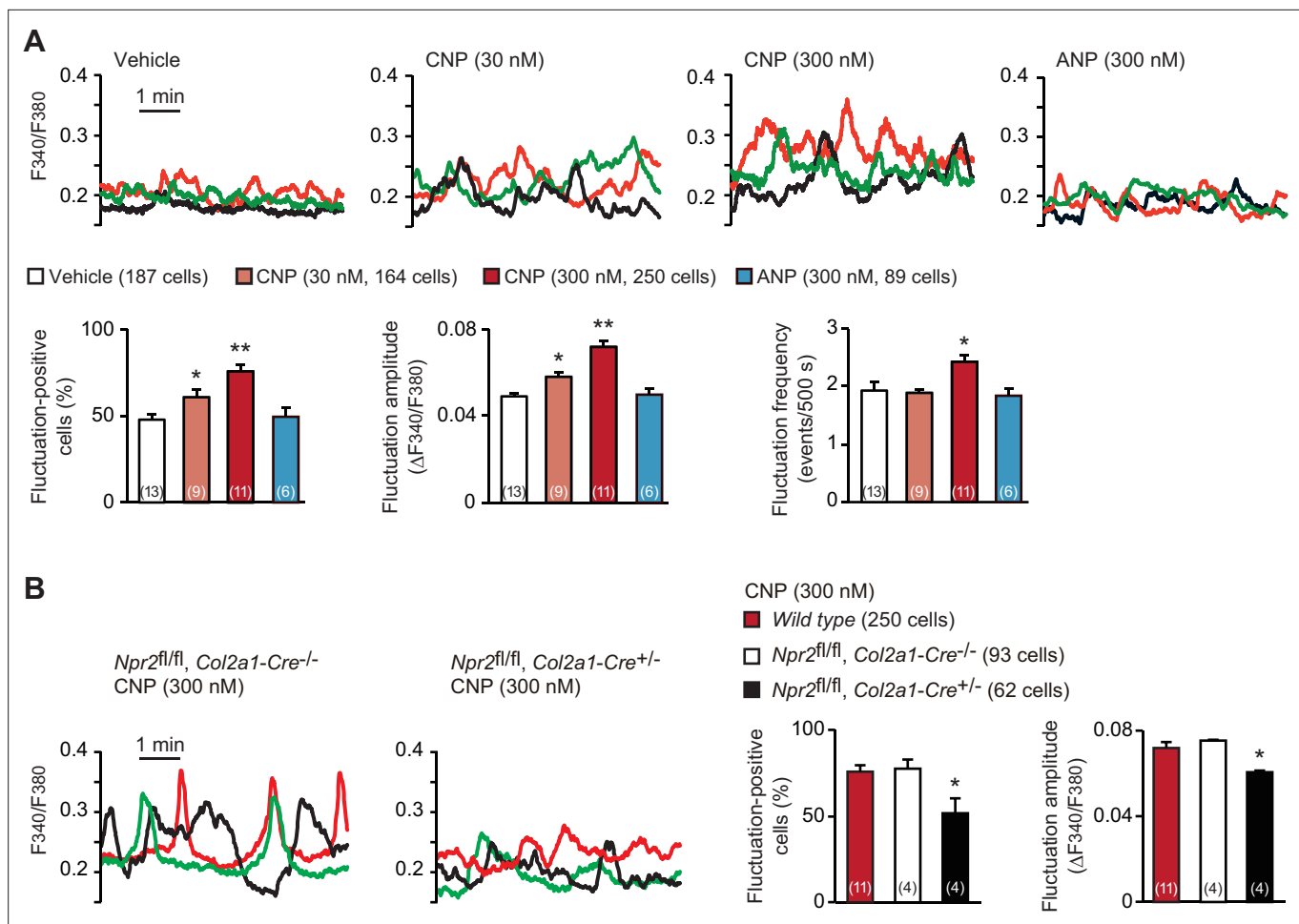


Figure 1. C-type natriuretic peptide (CNP)-induced facilitation of Ca^{2+} fluctuations in growth plate chondrocytes. **(A)** Fura-2 imaging of round chondrocytes pretreated with or without natriuretic peptides. Femoral bone slices prepared from wild-type C57BL embryos were pretreated with or without CNP and atrial natriuretic peptide (ANP), and subjected to Ca^{2+} imaging. Representative recording traces from three cells are shown in each pretreatment group (upper panels). The effects of CNP and ANP pretreatments on spontaneous Ca^{2+} fluctuations are summarized (lower graphs). The fluctuation-positive cell ratio, fluctuation amplitude and frequency were statistically analyzed, and significant differences from the control vehicle pretreatment are marked with asterisks (* $p < 0.05$ and ** $p < 0.01$ in one-way analysis of variance (ANOVA) and Dunnett's test). The data are presented as the means \pm standard error of the mean (SEM), with n values indicating the number of examined mice. **(B)** Fura-2 imaging of round chondrocytes prepared from chondrocyte-specific *Npr2*-knockout (*Npr2^{fl/fl}, Col2a1-Cre^{-/-}*) and control (*Npr2^{fl/fl}, Col2a1-Cre^{+/-}*) mice. The bone slices were pretreated with CNP, and then subjected to Ca^{2+} imaging. Representative recording traces are shown (left panels) and the CNP-pretreated effects are summarized (right graphs); significant differences from the wild-type group are marked with asterisks (* $p < 0.05$ in one-way ANOVA and Tukey's test). The data are presented as the means \pm SEM with n values indicating the number of examined mice.

The online version of this article includes the following source data and figure supplement(s) for figure 1:

Source data 1. Related to **Figure 1A**.

Source data 2. Related to **Figure 1B**.

Figure supplement 1. Chondrocyte-specific *Npr2* ablation.

Figure supplement 1—source data 1. Related to **Figure 1—figure supplement 1B**.

Figure supplement 1—source data 2. Related to **Figure 1—figure supplement 1B**.

Figure supplement 1—source data 3. Related to **Figure 1—figure supplement 1C**.

Figure supplement 1—source data 4. Related to **Figure 1—figure supplement 1D**.

Figure supplement 2. Gene expression analysis in wild-type growth plate chondrocytes.

Figure supplement 2—source data 1. Related to **Figure 1—figure supplement 2**.

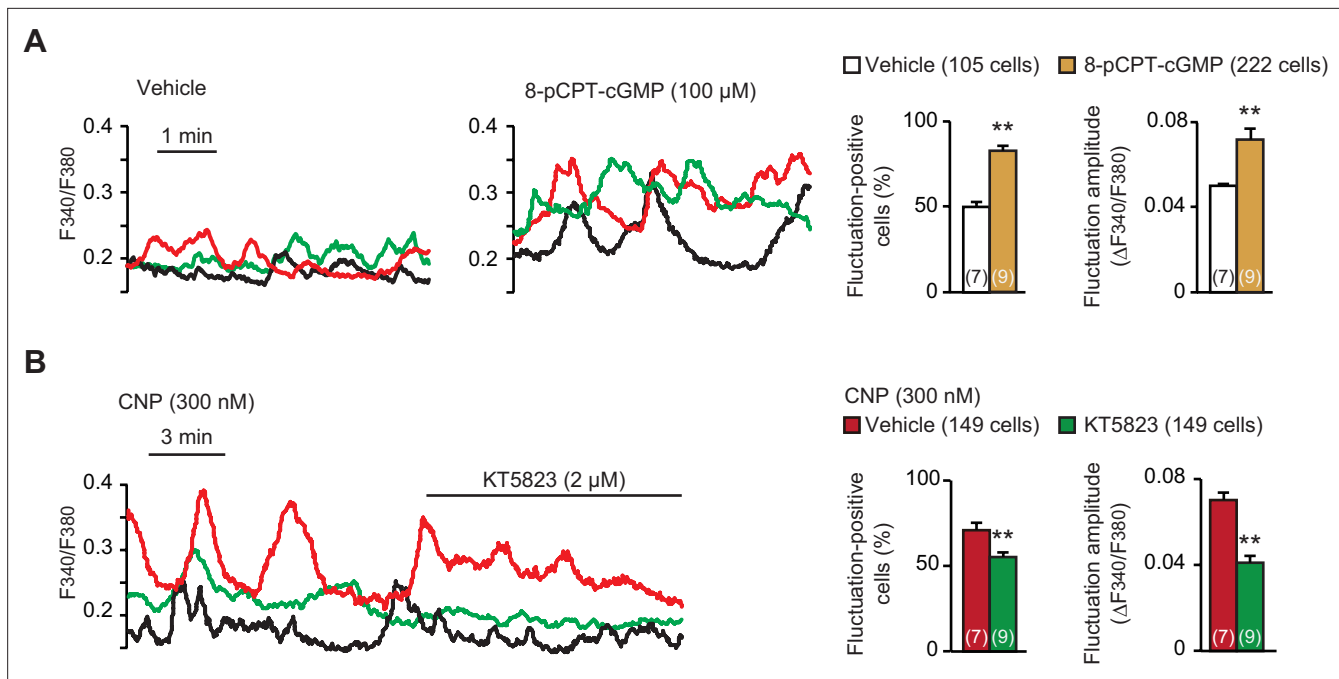


Figure 2. Contribution of cGMP-dependent protein kinase (PKG) to C-type natriuretic peptide (CNP)-facilitated Ca^{2+} fluctuations. **(A)** Facilitated Ca^{2+} fluctuations in round chondrocytes pretreated with the PKG activator 8-pCPT-cGMP. Wild-type bone slices were pretreated with or without the cGMP analog, and then subjected to Ca^{2+} imaging. Representative recording traces are shown (left panels), and the pharmacological effects are summarized (right graphs). Significant differences between control and 8-pCPT-cGMP pretreatments are marked with asterisks (** $p < 0.01$ in t -test). The data are presented as the means \pm standard error of the mean (SEM) with n values indicating the number of examined mice. **(B)** Attenuation of CNP-facilitated Ca^{2+} fluctuations by the PKG inhibitor KT5823. Wild-type bone slices were pretreated with CNP, and then subjected to Ca^{2+} imaging. Representative recording traces are shown (left panel), and KT5823-induced effects are summarized (right graphs). Significant KT5823-induced shifts are marked with asterisks (** $p < 0.01$ in t -test). The data are presented as the means \pm SEM with n values indicating the number of examined mice.

The online version of this article includes the following source data for figure 2:

Source data 1. Related to **Figure 2A**.

Source data 2. Related to **Figure 2B**.

of representative chondrogenic marker genes between chondrocyte-specific *Npr2*-knockout and control bones, suggesting that the *Npr2* deficiency does not affect fundamental chondrogenesis in growth plates (**Figure 1—figure supplement 1D**). In contrast to the imaging observations in wild-type and control bone slices, CNP treatments failed to enhance Ca^{2+} fluctuations in the mutant round chondrocytes prepared from the chondrocyte-specific *Npr2*-knockout mice (**Figure 1B**). Therefore, CNP seems to facilitate spontaneous Ca^{2+} fluctuations downstream of NPR2 activation in growth plate chondrocytes.

Activated PKG facilitates spontaneous Ca^{2+} fluctuations

CNP binds to NPR2 to activate its intrinsic guanylate cyclase and thus stimulates PKG by elevating cellular cGMP contents (Nakao *et al.*, 1996). CNP also binds to NPR3 which acts as a decoy receptor for ligand clearance, but the *Npr3* gene seemed to be inactive in growth plate chondrocytes (**Figure 1—figure supplement 2**). Next, we pharmacologically verified the contribution of PKG to CNP-facilitated Ca^{2+} fluctuations. The cGMP analog 8-(4-chlorophenylthio)-cyclic GMP (8-pCPT-cGMP) is widely used as a PKG-selective activator, while KT5823 is a typical PKG inhibitor. In wild-type growth plate chondrocytes pretreated with 8-pCPT-cGMP (100 μM for 1 hr), spontaneous Ca^{2+} fluctuations were remarkably facilitated (**Figure 2A**); both fluctuation-positive cell rate and fluctuation amplitude were highly increased. In contrast, the bath application of KT5823 (2 μM) clearly attenuated CNP-facilitated Ca^{2+} fluctuations within a short time frame (**Figure 2B**). Therefore, PKG activation seems to be essential for CNP-facilitated Ca^{2+} fluctuations in growth plate chondrocytes.

Activated BK channels contribute to CNP-facilitated Ca²⁺ fluctuations

Spontaneous Ca²⁺ fluctuations are facilitated by activated BK channels in growth plate chondrocytes (Qian *et al.*, 2019). Previous studies have established a functional link between PKG and BK channels in several cell types including smooth muscle and endothelial cells; activated PKG enhances BK channel gating by directly phosphorylating the α subunit KCNMA1 protein (Dong *et al.*, 2008; Fukao *et al.*, 1999; White *et al.*, 2000). We thus examined whether altered BK channel activity is associated with CNP-facilitated Ca²⁺ fluctuations. The BK channel inhibitor paxilline (10 μ M) exerted no obvious effects on basal Ca²⁺ fluctuations in nontreated chondrocytes. However, the same paxilline treatments remarkably inhibited CNP-facilitated Ca²⁺ fluctuations (Figure 3A); both fluctuation-positive cell ratio and fluctuation amplitude were clearly decreased after paxilline application. On the other hand, the BK channel activator NS1619 (30 μ M) stimulated basal Ca²⁺ fluctuations in the growth plate chondrocytes prepared from control mice. The NS1619-induced effects were preserved in the mutant chondrocytes prepared from chondrocyte-specific *Npr2*-knockout mice (Figure 3B). Therefore, BK channel activation is likely involved in CNP-facilitated Ca²⁺ fluctuations in growth plate chondrocytes.

Phospholipase C seems unrelated to CNP-facilitated Ca²⁺ fluctuations

Ca²⁺ fluctuations are maintained by phosphatidylinositol (PI) turnover in growth plate chondrocytes (Qian *et al.*, 2019). Although it has been reported that activated PKG inhibits phospholipase C (PLC) in smooth muscle (Guo *et al.*, 2018; Huang *et al.*, 2007; Nalli *et al.*, 2014; Xia *et al.*, 2001), it might be possible that NPR2 activation enhances basal PLC activity to facilitate Ca²⁺ fluctuations. The PLC inhibitor U73122 (10 μ M) remarkably inhibited basal Ca²⁺ fluctuations in nontreated chondrocytes: the fluctuation-positive cell ratio and fluctuation amplitude reduced less than half in response to U73122 application (Figure 3—figure supplement 1). U73122 was also effective for CNP-facilitated Ca²⁺ fluctuations, but the inhibitory efficiency seemed relatively weak compared to those on basal fluctuations. Given the different inhibitory effects, it is rather unlikely that PLC activation accompanies CNP-facilitated Ca²⁺ fluctuations.

PKG stimulates sarco/endoplasmic reticulum Ca²⁺-ATPase (SERCA) by phosphorylating the Ca²⁺ pump regulatory peptide phospholamban (PLN) in smooth and cardiac muscle cells (Bibli *et al.*, 2015; Raeymaekers *et al.*, 1988; Lalli *et al.*, 1999), and activated Ca²⁺ pumps generally elevate stored Ca²⁺ contents and thus stimulate store Ca²⁺ release. RT-PCR data suggested that the *Pln* gene and the *Atp2a2* gene encoding SERCA2 are weakly active in growth plate chondrocytes (Figure 1—figure supplement 2). To examine the effects of CNP treatments on Ca²⁺ stores, we examined Ca²⁺ responses to the activation of Gq-coupled lysophosphatidic acid (LPA) receptors (Figure 3—figure supplement 2A) and the Ca²⁺ pump inhibitor thapsigargin (Figure 3—figure supplement 2B). CNP- and vehicle-pretreated chondrocytes exhibited similar LPA-induced Ca²⁺ release and thapsigargin-induced Ca²⁺ leak responses. Therefore, CNP treatments seem ineffective for store Ca²⁺ pumps in growth plate chondrocytes. Moreover, the dose dependency of Ca²⁺ release by LPA (1–10 μ M) was not altered between CNP- and vehicle-pretreated chondrocytes, implying that CNP does not affect basal PLC activity.

Among diverse Ca²⁺ handling-related proteins, PLC, PLN, and BK channels have been reported as PKG substrates, however, our observations suggested that both PLC and PLN receive no obvious functional regulation in CNP-treated chondrocytes. On the other hand, the paxilline treatments diminished CNP-facilitated Ca²⁺ fluctuations down to nontreated basal levels (Figure 3A), suggesting that activated BK channels predominantly contribute to CNP-facilitated Ca²⁺ fluctuations in growth plate chondrocytes.

CNP induces BK channel-mediated hyperpolarization

To confirm the contribution of activated BK channels to CNP-facilitated Ca²⁺ fluctuations, we conducted confocal imaging using the voltage-dependent dye oxonol VI. In this imaging analysis, depolarization results in the accumulation of the dye into cells, in which the fractional fluorescence intensity, normalized to the maximum intensity monitored in the bath solution containing 100 mM KCl, is thus increased (Figure 4A, left panel). The fractional intensity of CNP-pretreated cells was significantly lower than that of nontreated cells in a normal bath solution (Figure 4A, middle graph), although both cells exhibited similar intensity shifts in high K⁺ bath solutions. Based on the recording data, we prepared a calibration plot for the relationship between the fractional intensity and theoretical

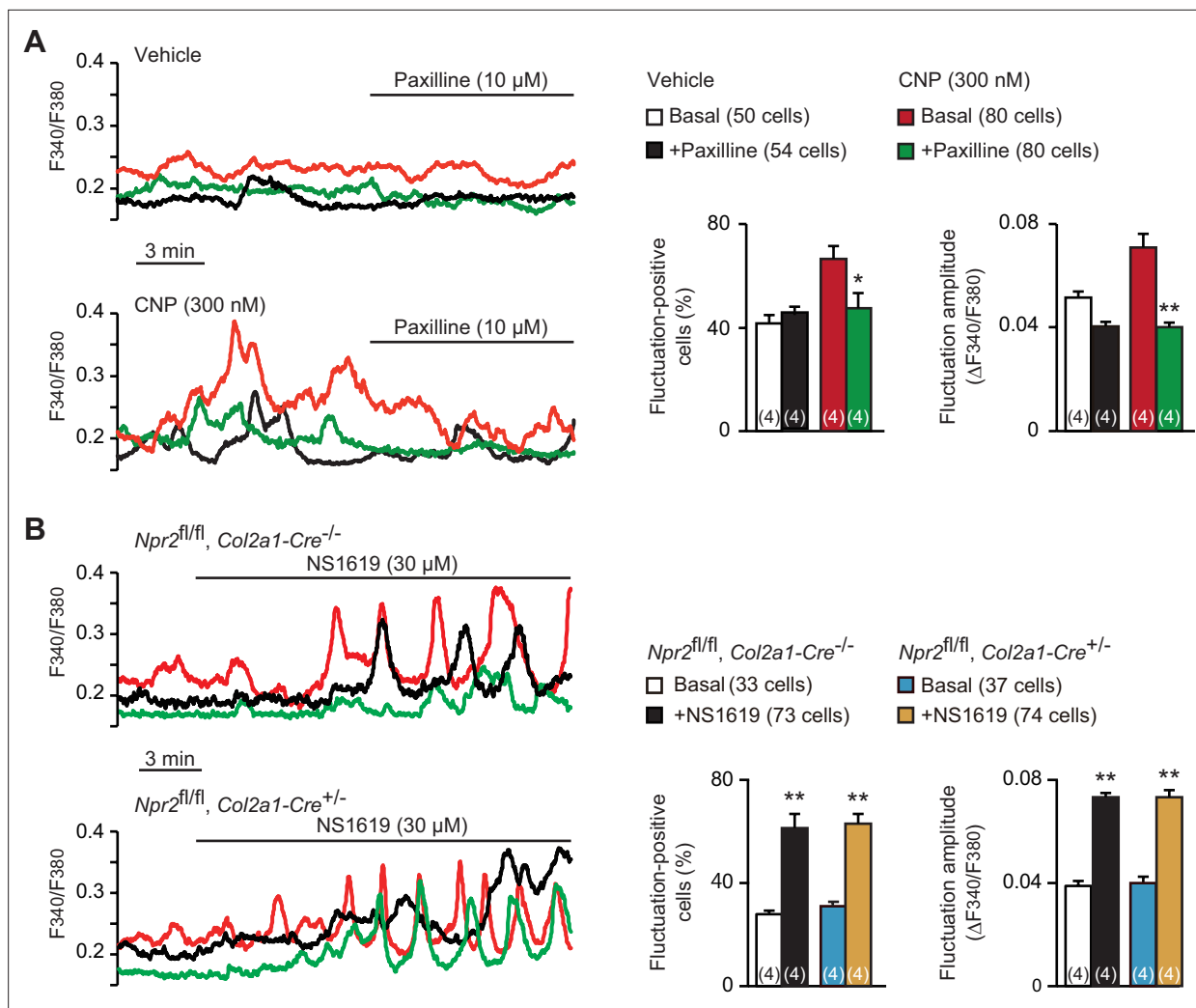


Figure 3. Contribution of BK channels to C-type natriuretic peptide (CNP)-facilitated Ca²⁺ fluctuations. **(A)** Attenuation of CNP-facilitated Ca²⁺ fluctuations by the BK channel inhibitor paxilline in round chondrocytes. Wild-type bone slices were pretreated with or without CNP, and then subjected to Ca²⁺ imaging. Representative recording traces are shown (left panels), and paxilline-induced effects are summarized (right graphs). Significant paxilline-induced shifts are marked with asterisks (*p < 0.05 and **p < 0.01 in one-way analysis of variance (ANOVA) and Tukey's test). The data are presented as the means ± standard error of the mean (SEM) with n values indicating the number of examined mice. **(B)** Ca²⁺ fluctuations facilitated by the BK channel activator NS1619 in *Npr2*-deficient chondrocytes. Bone slices were prepared from the chondrocyte-specific *Npr2*-knockout and control embryos, and NS1619-induced effects were examined in Ca²⁺ imaging. Representative recording traces are shown (left panels), and the effects of NS1619 are summarized (right graphs). Significant NS1619-induced shifts are marked with asterisks (**p < 0.01 in one-way ANOVA and Tukey's test). The data are presented as the means ± SEM with n values indicating the number of examined mice.

The online version of this article includes the following source data and figure supplement(s) for figure 3:

Source data 1. Related to **Figure 3A**.

Source data 2. Related to **Figure 3B**.

Figure supplement 1. Effects of phospholipase C (PLC) inhibitor U73122 on C-type natriuretic peptide (CNP)-facilitated Ca²⁺ fluctuations.

Figure supplement 1—source data 1. Related to **Figure 3—figure supplement 1**.

Figure supplement 2. Store Ca²⁺ release in C-type natriuretic peptide (CNP)-treated round chondrocytes.

Figure supplement 2—source data 1. Related to **Figure 3—figure supplement 2A**.

Figure supplement 2—source data 2. Related to **Figure 3—figure supplement 2B**.

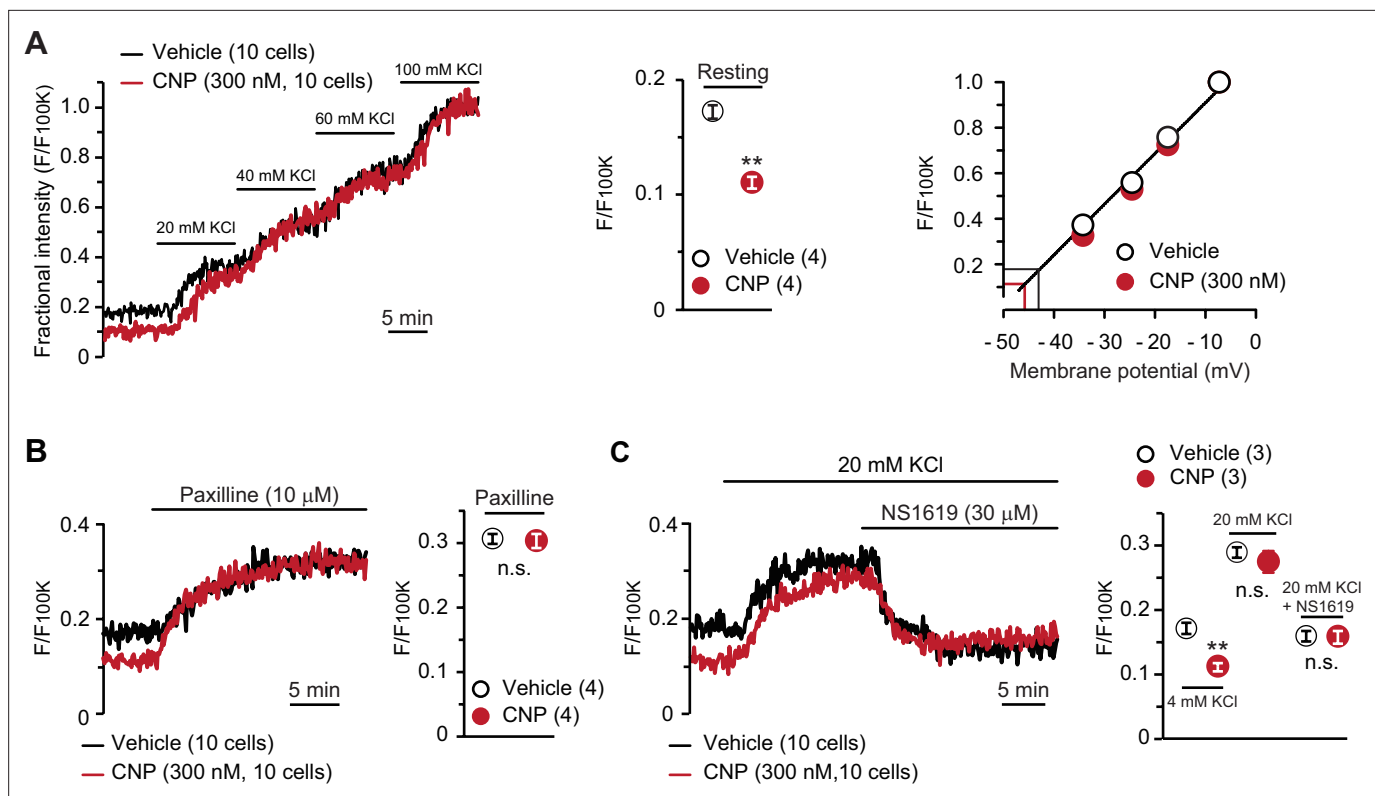


Figure 4. BK channel-mediated hyperpolarization induced by C-type natriuretic peptide (CNP). **(A)** Oxonol VI imaging of round chondrocytes pretreated with or without CNP. Wild-type bone slices were pretreated with or without CNP, and then subjected to membrane potential imaging. During contiguous treatments with high-K⁺ solutions, cellular fluorescence intensities were monitored and normalized to the maximum value in the 100 mM KCl-containing solution to yield the fractional intensity (left panel). The resting fractional intensities were quantified and statistically analyzed in CNP- and vehicle-pretreated cells (middle graph). For preparing the calibration plot (right panel), the data from 10 cells in bathing solutions containing 4 (normal solution), 20, 40, 60, and 100 mM KCl are summarized; red and black lines indicate the estimated resting membrane potentials of CNP- and vehicle-pretreated cells, respectively. **(B)** Effects of the BK channel inhibitor paxilline on resting membrane potential in round chondrocytes. Recording data from 10 cells pretreated with or without CNP were averaged (left panel), and the fractional intensities elevated by paxilline are summarized (right graph). **(C)** Effects of the BK channel activator NS1619 on membrane potential in round chondrocytes. Recording data from 10 cells pretreated with or without CNP were averaged (left panel), and the fractional intensities in normal, 20 mM KCl and NS1619-containing 20 mM KCl solutions are summarized (right graph). Significant differences between CNP- and vehicle-pretreated cells are indicated by asterisks in **(A)** (***p* < 0.01 in *t*-test) and in **(C)** (***p* < 0.01 in one-way analysis of variance [ANOVA] and Dunn's test). The data are presented as the means ± standard error of the mean (SEM) with *n* values indicating the number of examined mice.

The online version of this article includes the following source data for figure 4:

Source data 1. Related to **Figure 4A**.

Source data 2. Related to **Figure 4B**.

Source data 3. Related to **Figure 4C**.

membrane potential (**Figure 4A**, right panel). In the tentative linear correlation, resting potentials of -46.4 ± 0.2 and -43.6 ± 0.3 mV were estimated in CNP- and nontreated cells, respectively. The estimated potentials closely approximate the reported value from monitoring articular chondrocytes using sharp microelectrodes (*Clark et al., 2010*).

In pharmacological assessments, paxilline elevated fractional intensities to the same levels in CNP- and nontreated chondrocytes (**Figure 4B**). Moreover, NS1619 decreased fractional intensities to the same levels in both cells under 20 mM KCl bathing conditions, which enabled us to reliably evaluate the reducing intensity shifts (**Figure 4C**). The oxonol VI imaging data suggested that CNP treatments induce BK channel-mediated hyperpolarization and thus facilitate spontaneous Ca²⁺ fluctuations by enhancing Ca²⁺-driving forces in growth plate chondrocytes.

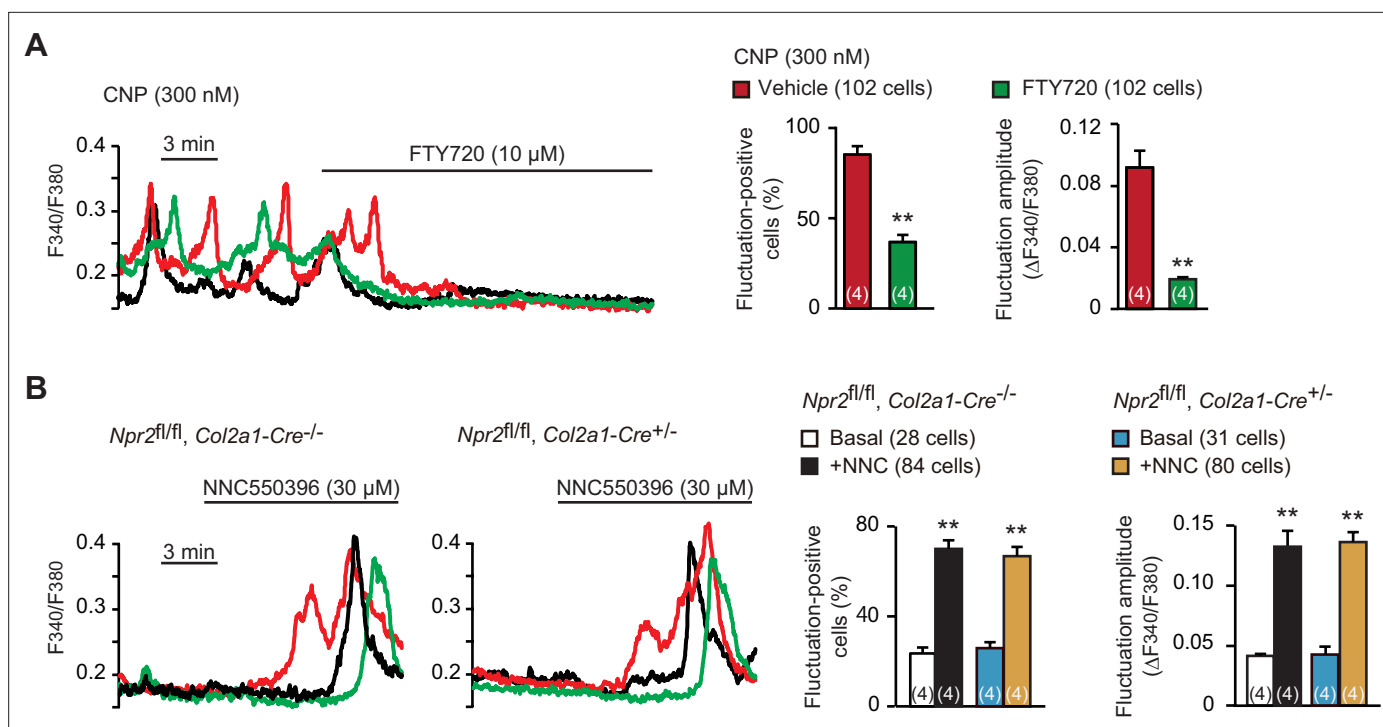


Figure 5. Enhanced TRPM7-mediated Ca²⁺ entry by C-type natriuretic peptide (CNP) treatments. **(A)** Inhibition of CNP-facilitated Ca²⁺ fluctuations by the TRPM7 inhibitor FTY720 in round chondrocytes. Wild-type bone slices were pretreated with CNP, and then subjected to Ca²⁺ imaging. Representative recording traces are shown (left panel), and the effects of FTY720 are summarized (right graphs). Significant FTY720-induced shifts are marked with asterisks (***p* < 0.01 in *t*-test). The data are presented as the means ± standard error of the mean (SEM) with *n* values indicating the number of examined mice. **(B)** Ca²⁺ fluctuations facilitated by the TRPM7 channel activator NNC550396 in *Npr2*-deficient round chondrocytes. Bone slices were prepared from the chondrocyte-specific *Npr2*-knockout and control embryos, and NNC550396-induced effects were examined in Ca²⁺ imaging. Representative recording traces are shown (left panels) and the effects of NNC550396 on Ca²⁺ fluctuations are summarized (right graphs). Significant NNC550396-induced shifts in each genotype are marked with asterisks (***p* < 0.01 in one-way analysis of variance [ANOVA] and Tukey's test). The data are presented as the means ± SEM with *n* values indicating the number of examined mice.

The online version of this article includes the following source data for figure 5:

Source data 1. Related to **Figure 5A**.

Source data 2. Related to **Figure 5B**.

CNP enhances TRPM7-mediated Ca²⁺ entry and CaMKII activity

Spontaneous Ca²⁺ fluctuations are predominantly attributed to the intermissive gating of cell-surface TRPM7 channels in growth plate chondrocytes (Qian *et al.*, 2019). For pharmacological characterization of TRPM7 channels, FTY720 is used as a typical inhibitor, while NNC550396 is an activator. As reasonably expected, bath application of FTY720 (10 μM) clearly diminished CNP-facilitated Ca²⁺ fluctuations (Figure 5A). On the other hand, NNC550396 (30 μM) remarkably facilitated Ca²⁺ fluctuations in nontreated chondrocytes, and this facilitation was preserved in the mutant chondrocytes prepared from chondrocyte-specific *Npr2*-knockout mice (Figure 5B). Therefore, CNP treatments likely facilitate TRPM7-mediated Ca²⁺ influx in growth plate chondrocytes.

TRPM7-mediated Ca²⁺ entry activates CaMKII in growth plate chondrocytes toward bone outgrowth (Qian *et al.*, 2019), and cellular CaMKII activity can be estimated by immunocytochemically quantifying its autophosphorylated form. In immunocytochemical analysis, CNP-pretreated growth plate chondrocytes were more decorated with the antibody against phospho-CaMKII than nontreated control cells (Figure 6A). This CNP-facilitated decoration was abolished by the cotreatment of the CaMKII inhibitor KN93 (30 μM). This observation was further confirmed by Western blot analysis; CNP treatments increased the phospho-CaMKII population without affecting total CaMKII content in the cell lysates prepared from growth plates (Figure 6B). Therefore, CaMKII is likely activated downstream of enhanced TRPM7-mediated Ca²⁺ entry in CNP-treated growth plate chondrocytes.

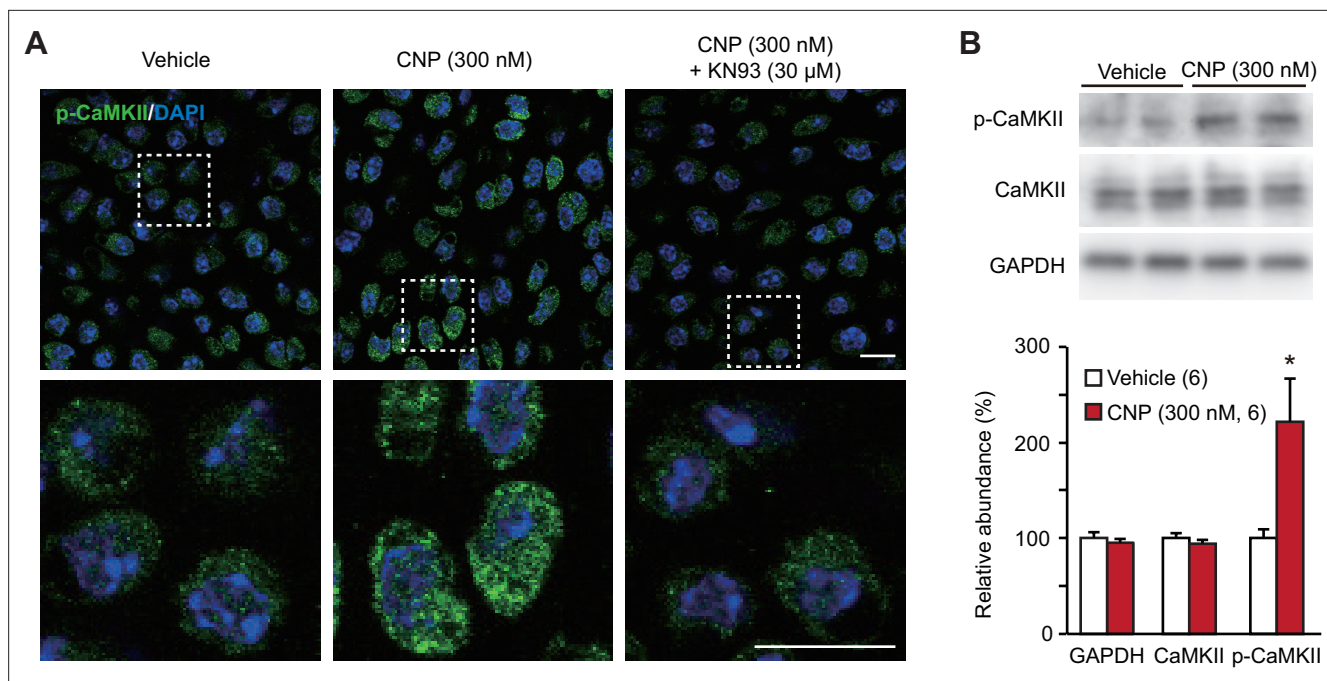


Figure 6. CaMKII activation in C-type natriuretic peptide (CNP)-treated round chondrocytes. **(A)** Immunohistochemical staining against phospho-CaMKII (p-CaMKII) in round chondrocytes. Wild-type bone slices were pretreated with or without CNP and the CaMKII inhibitor KN93, and then subjected to immunostaining with antibody to p-CaMKII. DAPI (4',6-diamidino-2-phenylindole) was used for nuclear staining. Lower panels show high-magnification views of white-dotted regions in upper panels (scale bars, 10 μ m). **(B)** Immunoblot analysis of total CaMKII and p-CaMKII in growth plate cartilage. Growth plate lysates were prepared from wild-type bone slices pretreated with or without CNP, and subjected to immunoblot analysis with antibodies against total CaMKII and p-CaMKII (upper panel). Glyceraldehyde-3-phosphate dehydrogenase (GAPDH) was also analyzed as a loading control. The immunoreactivities observed were densitometrically quantified and are summarized (lower graph). A significant difference between CNP- and vehicle pretreatments is marked with an asterisk (* $p < 0.05$ in one-way analysis of variance [ANOVA] and Tukey's test). The data are presented as the means \pm standard error of the mean (SEM) with n values indicating the number of examined mice.

The online version of this article includes the following source data for figure 6:

Source data 1. Related to **Figure 6B**.

Source data 2. Related to **Figure 6B**.

Pharmacologically activated BK channels facilitate bone outgrowth

Based on the present data from *in vitro* experiments, the novel CNP signaling route, represented as the NPR2-PKG-BK channel-TRPM7 channel-CaMKII axis, can be proposed in growth plate chondrocytes. We attempted to examine the proposed signaling axis in metatarsal bone culture, a widely used *ex vivo* model system for analyzing bone growth and endochondral ossification (Houston *et al.*, 2016). CNP treatments expanded columnar chondrocytic zones without affecting cell densities to extend cultured wild-type metatarsal bones (**Figure 7—figure supplement 1**). The extension seemed to be mainly caused by enlarged extracellular matrix area, although CNP significantly dilated columnar cell sizes. In chondrocyte-specific *Trpm7*-knockout mice (*Trpm7^{fl/fl}*, *Col11a2-Cre^{+/-}*), Cre recombinase is expressed under the control of the collagen type XI gene enhancer and promoter, and thus inactivates the floxed *Trpm7* alleles in cartilage cells (Qian *et al.*, 2019). The bone rudiments prepared from control embryos (*Trpm7^{fl/fl}*, *Col11a2-Cre^{-/-}*) regularly elongated during *ex vivo* culture, and their outgrowth was significantly stimulated by the supplementation with CNP (30 nM) into the culture medium (**Figure 7A**). The histological observation of the growth plate regions demonstrated that the CNP treatment extended the columnar chondrocyte zone. In contrast, the mutant rudiments prepared from the chondrocyte-specific *Trpm7*-knockout embryos were reduced in initial size and did not respond to the CNP supplementation (**Figure 7B**). Therefore, CNP-facilitated bone outgrowth seems to require TRPM7 channels expressed in growth plate chondrocytes.

In our proposed signaling axis, activated BK channels exert an essential role by converting the chemical signal into the electrical signal. We finally examined the effect of the BK channel activator

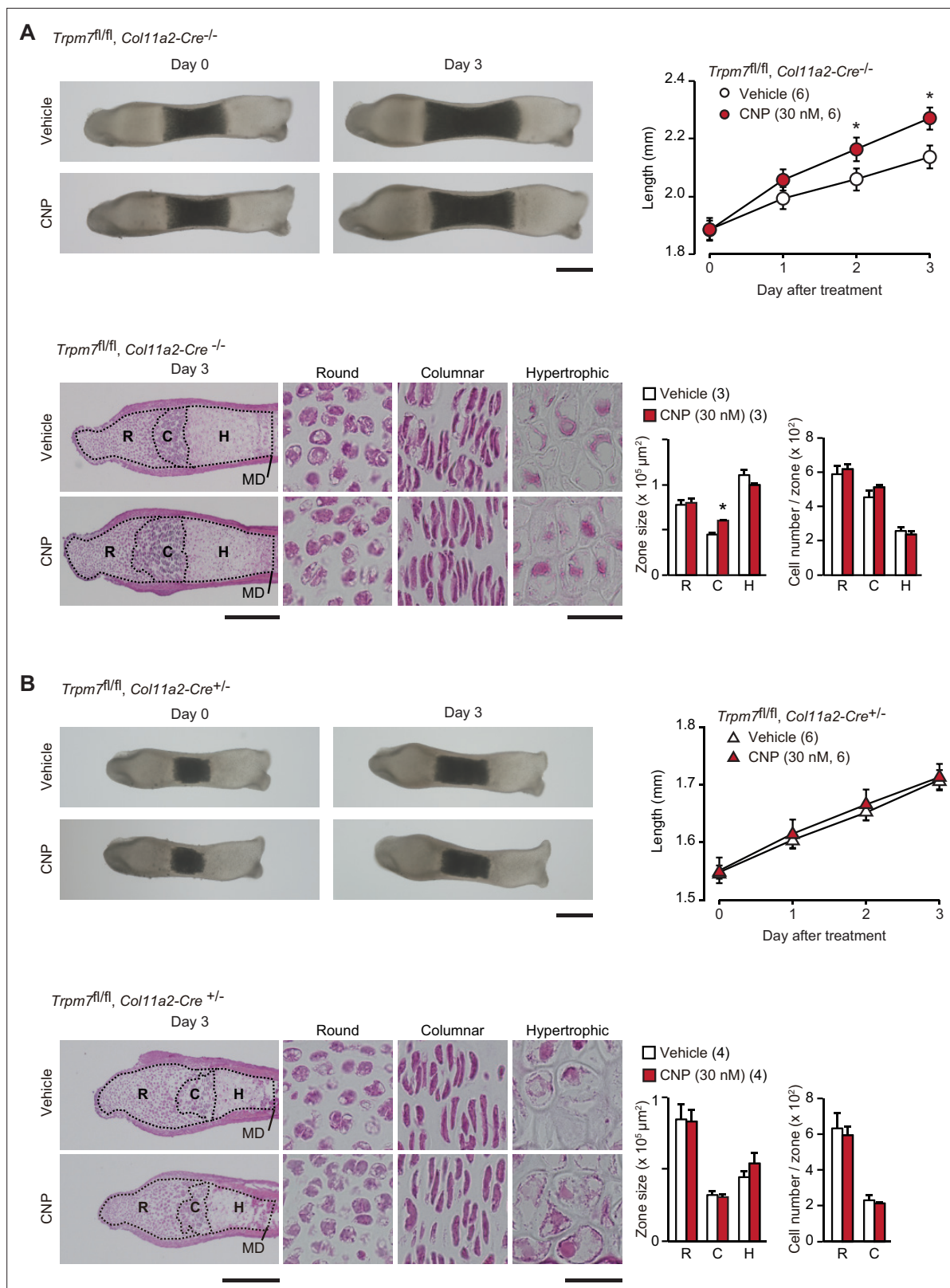


Figure 7. Contribution of TRPM7 channel to C-type natriuretic peptide (CNP)-facilitated bone outgrowth. Loss of CNP-facilitated outgrowth in *Trpm7*-deficient bones. Metatarsal rudiments isolated from control (*Trpm7^{fl/fl}, Col11a2-Cre^{-/-}*) embryos (A) and chondrocyte-specific *Trpm7*-knockout (*Trpm7^{fl/fl}, Col11a2-Cre^{+/-}*) embryos (B) were precultured in normal medium for 6 days, and then cultured in medium supplemented with or without CNP for 3 days. Representative images of cultured metatarsals are shown (upper left panels; scale bar, 0.3 mm), and longitudinal bone outgrowth during the

Figure 7 continued on next page

Figure 7 continued

CNP-supplemented period was statistically analyzed in each genotype group (upper right graphs). Growth plate images in longitudinal sections of 3-day cultured bones with or without CNP treatments are presented in lower left panels (scale bar, 0.3 mm), and their high-magnification views in the round (R), columnar (C), and hypertrophic (H) chondrocyte zones are shown in lower right panels (scale bar, 30 μ m). MD, mid-diaphysis. Summary of graphical representations of zonal sizes containing round, columnar, and hypertrophic chondrocytes and number of cells in each zone is shown in lower right graphs. Significant CNP-supplemented effects are marked with asterisks (* $p < 0.05$ in t-test). The data are presented as the means \pm standard error of the mean (SEM) with n values indicating the number of examined mice.

The online version of this article includes the following source data and figure supplement(s) for figure 7:

Source data 1. Related to **Figure 7A**.

Source data 2. Related to **Figure 7B**.

Figure supplement 1. Histological analysis of metatarsal bones treated with C-type natriuretic peptide (CNP).

Figure supplement 1—source data 1. Related to **Figure 7—figure supplement 1**.

Figure supplement 2. Proposed C-type natriuretic peptide (CNP)-evoked signaling in growth plate chondrocytes.

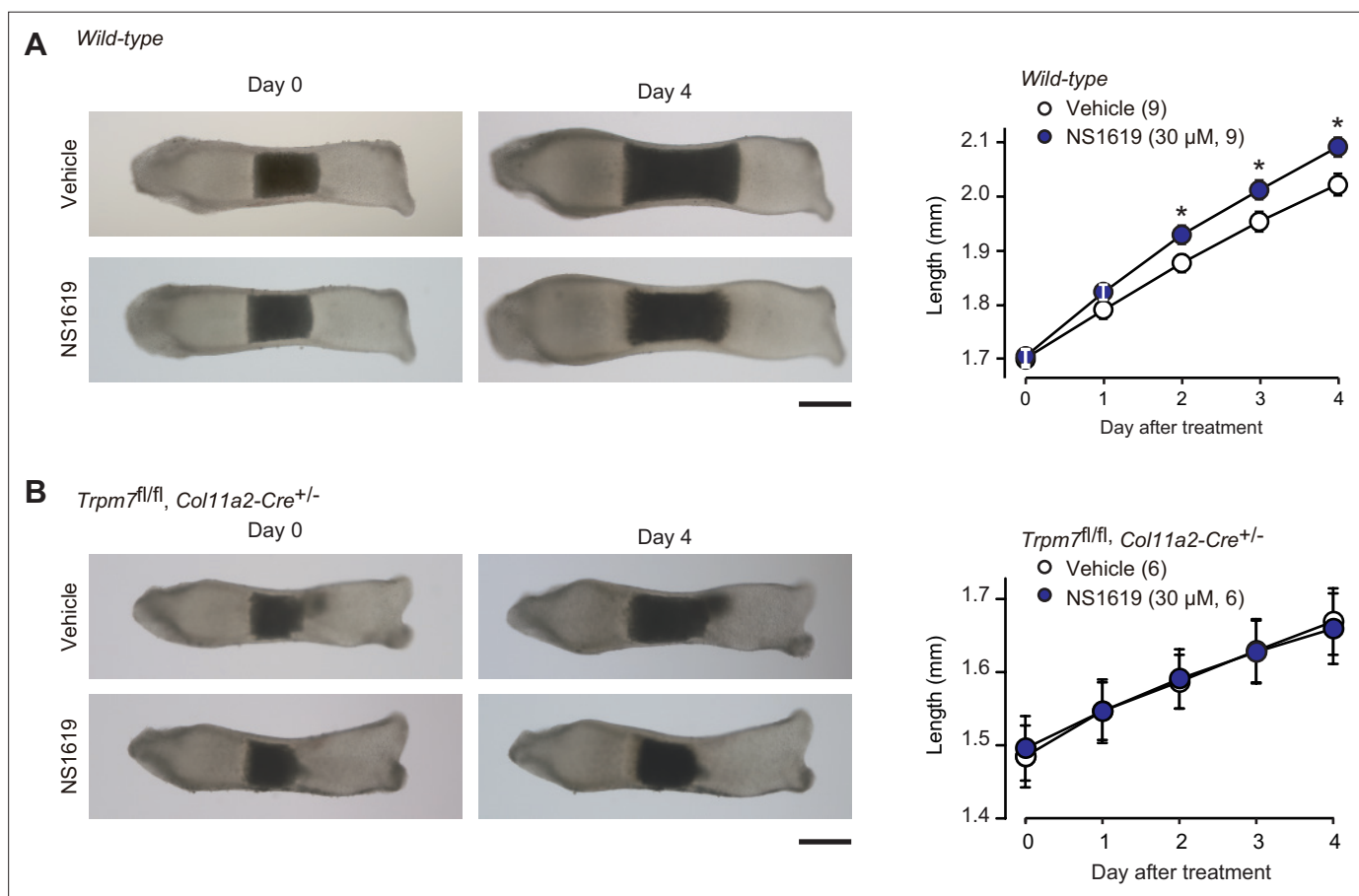


Figure 8. Facilitated bone outgrowth by BK channel activator. Stimulated bone outgrowth by the BK channel activator NS1619. Metatarsal rudiments isolated from wild-type (**A**) and the chondrocyte-specific *Trpm7*-knockout embryos (**B**) were precultured in normal medium for 5 days, and then cultured in medium supplemented with or without NS1619 for 4 days. Representative images of cultured metatarsals are shown (left panels; scale bar, 0.3 mm), and longitudinal bone outgrowth during the NS1619-supplemented period was statistically analyzed in each genotype group (right graphs). A significant NS1619-supplemented effect is marked with asterisks (* $p < 0.05$ in t-test). The data are presented as the means \pm standard error of the mean (SEM) with n values indicating the number of examined mice.

The online version of this article includes the following source data for figure 8:

Source data 1. Related to **Figure 8A**.

Source data 2. Related to **Figure 8B**.

NS1619 on bone outgrowth (**Figure 8A**). NS1619 supplementation (30 μM) significantly stimulated the outgrowth of wild-type bone rudiments. In contrast, under the same culture conditions, no stimulation was detected in the mutant rudiments from the chondrocyte-specific *Trpm7*-deficient embryos (**Figure 8B**). The observations seem to support our conclusion that CNP activates BK channels and thus facilitates TRPM7-mediated Ca^{2+} influx in growth plate chondrocytes for stimulating bone outgrowth.

Discussion

We reported that in growth plate chondrocytes, PLC and BK channels maintain autonomic TRPM7-mediated Ca^{2+} fluctuations, which potentiate chondrogenesis and bone growth by activating CaMKII (**Qian et al., 2019**). Based on the present data, together with the previous reports, we proposed a new CNP signaling axis in growth plate chondrocytes (**Figure 7—figure supplement 2A**). CNP-induced NPR2 activation elevates cellular cGMP content and thus activates PKG, leading to the phosphorylation of BK channels. The resulting BK channel activation induces cellular hyperpolarization to facilitate TRPM7-mediated Ca^{2+} entry by enhancing the Ca^{2+} -driving force, leading to CaMKII activation. Therefore, it is likely that CaMKII activity is physiologically regulated by BK channels as a key player of the CNP signaling cascade. In a recent genetic study, several patients carrying loss-of-function mutations in the *KCNMA1* gene encoding BK channel α subunit were characterized by a novel syndromic growth deficiency associated with severe developmental delay, cardiac malformation, bone dysplasia, and dysmorphic features (**Liang et al., 2019**). In the *KCNMA1*-mutated disorder, CNP signaling likely fails to facilitate TRPM7-mediated Ca^{2+} fluctuations in growth plate chondrocytes and resulting insufficient Ca^{2+} entry may lead to systemic bone dysplasia associated with stunted growth plate cartilage. On the other hand, the origin of CNP may still be ambiguous in the signaling scheme. Transgenic mice overexpressing CNP in a chondrocyte-specific manner develop a prominent skeletal overgrowth phenotype, suggesting autocrine CNP signaling in developing bones (**Yasoda et al., 2004**). However, several genechip data in public databases indicate that prepro-CNP mRNA is abundantly expressed in the placenta among embryonic tissues (e.g., see the records under accession number GSE28277 in NCBI database). Therefore, it may be important to further examine which cell type primarily produces CNP to facilitate bone growth during embryonic development.

In our proposed CNP-signaling cascade, CaMKII is finally activated by TRPM7-mediated Ca^{2+} influx in both round and columnar chondrocytes. However, it is still unclear how activated CaMKII contributes to bone outgrowth. Our observations in cultured metatarsal bones suggest that CNP expanded the columnar chondrocyte zone by stimulating the cell growth and enlarging the extracellular matrix area toward bone extension (**Figure 7**). The observations are roughly consistent with the previous studies using cultured tibias treated with CNP (**Yasoda et al., 1998; Miyazawa et al., 2002**). Therefore, activated CaMKII by TRPM7-mediated Ca^{2+} influx probably phosphorylates key proteins controlling cell growth and extracellular matrix production in columnar chondrocytes.

From a physiological point of view, it is interesting to note that the proposed CNP signaling axis has clear overlap with the nitric oxide (NO) and ANP/BNP signaling cascades for vascular relaxation (**Martel et al., 2010; Zois et al., 2014; Kubacka et al., 2018**). In blood vessels, NO is produced by endothelial cells in response to various stimuli including shear stress and acetylcholine, and activates soluble guanylate cyclase in neighboring vascular smooth muscle cells. ANP and BNP are released from the heart in response to pathological stresses, such as atrial distension and pressure overload, and are delivered to activate the receptor guanylate cyclase NPR1 in vascular muscle. In either case, the resulting cGMP elevation followed by PKG activation induces BK channel-mediated hyperpolarization and thus inhibits L-type Ca^{2+} channel gating, leading to vascular dilation due to decreased Ca^{2+} entry into vascular muscle. Therefore, activated BK channels inhibit the voltage-dependent Ca^{2+} influx in vascular muscle cells regarded as excitable cells (**Figure 7—figure supplement 2B**). In contrast, activated BK channels reversely stimulate TRPM7-mediated Ca^{2+} entry in growth plate chondrocytes classified as nonexcitable cells, because the channel activity is voltage independently maintained by the intrinsic PI turnover rate.

CNP is an effective therapeutic reagent for achondroplasia and divergent short statures (**Yasoda et al., 2004; Ueda et al., 2016; Yamashita et al., 2020**), and the phase III clinical trial of CNP therapy is completed successfully (**Nakao et al., 1996**). The proteins contributing to the CNP signaling axis may be new pharmaceutical targets for developing medications; in addition to NPR2, BK, and TRPM7

channels are reasonably considered promising targets. Moreover, phosphodiesterase subtypes might be useful targets, although the subtypes responsible for cGMP hydrolysis remain to be identified in growth plate chondrocytes. Chemical compounds specifically targeting the signaling axis defined in this study would be useful drugs for not only clinical treatment of developmental disorders but also artificially modifying body sizes in farm and pet animals.

Materials and methods

Key resources table

Reagent type (species) or resource	Designation	Source or reference	Identifiers	Additional information
Strain, strain background (<i>Mus musculus</i>)	Mouse: C57BL/6J	The Jackson Laboratory	Jax: 000664	
Strain, strain background (<i>Mus musculus</i>)	<i>Trpm7^{fl/fl}, Col11a2-Cre</i> mice	Qian et al., 2019	N/A	
Strain, strain background (<i>Mus musculus</i>)	<i>Npr2^{fl/fl}, Col2a1-Cre</i> mice	Nakao et al., 2015	N/A	
Antibody	Anti-phospho-CaMKII (Thr 286) (Rabbit monoclonal)	Cell Signaling Technology	Cat#12716; RRID: AB_2713889	IF (1:200) WB (1:1000)
Antibody	Anti-CaMKII (Rabbit monoclonal)	Abcam	Cat#EP1829Y; RRID: AB_868641	WB (1:1000)
Antibody	Anti-GAPDH (Rabbit polyclonal)	Sigma-Aldrich	Cat#G9545; RRID: AB_796208	WB (1:10,000)
Antibody	Anti-rabbit IgG-HRP (Mouse monoclonal)	Santa Cruz	Cat#sc-2357; RRID: AB_628497	1:2000
Antibody	Anti-rabbit Alexa Flour 488 (Goat polyclonal)	Invitrogen	Cat#A-11008; RRID: AB_143165	1:50
Sequence-based reagent	Mouse <i>Npr1_F</i>	This paper	PCR primers	AACAAGGAGAACAGCAGCAAC
Sequence-based reagent	Mouse <i>Npr1_R</i>	This paper	PCR primers	TATCAAATGCCTCAGCCTGGA
Sequence-based reagent	Mouse <i>Npr2_F</i>	This paper	PCR primers	GGCCCCATCCCTGATGAAC
Sequence-based reagent	Mouse <i>Npr2_R</i>	This paper	PCR primers	CCTGGTACCCCTTCTGTGA
Sequence-based reagent	Mouse <i>Npr3_F</i>	This paper	PCR primers	GGTATGGGGACTTCTCTGTG
Sequence-based reagent	Mouse <i>Npr3_R</i>	This paper	PCR primers	TCTGGTCTCATCTAGTCTCA
Sequence-based reagent	FIFor	This paper	PCR primers	GTAACCTGGGTAGACTAGTTGTTGG
Sequence-based reagent	DelFor	This paper	PCR primers	TGTTATTTGTGAGATGACG
Sequence-based reagent	Rev	This paper	PCR primers	ATGGTGAGGAGGTCTTTAATTCC
Sequence-based reagent	<i>Col2a1-Cre_F</i>	This paper	PCR primers	CGTTGTGAGTTGGATAGTTG
Sequence-based reagent	<i>Col2a1-Cre_R</i>	This paper	PCR primers	CATTGCTGTCACTTGGTCGT
Sequence-based reagent	Mouse <i>Prkg1_F</i>	This paper	PCR primers	ATGGACTTTTTGTGGGACTC
Sequence-based reagent	Mouse <i>Prkg1_R</i>	This paper	PCR primers	GGTTTTTCATTGGATCTGGGC
Sequence-based reagent	Mouse <i>Prkg2_F</i>	This paper	PCR primers	TTGCGGAAGAAAATGATGTCG
Sequence-based reagent	Mouse <i>Prkg2_R</i>	This paper	PCR primers	GAATGGGGAGGTTGAGGAGAA

Continued on next page

Continued

Reagent type (species) or resource	Designation	Source or reference	Identifiers	Additional information
Sequence-based reagent	Mouse <i>Kcnma_F</i>	<i>Liu et al., 2021</i>	PCR primers	AATGCACTTCGAGGAGGCTA
Sequence-based reagent	Mouse <i>Kcnma_R</i>	<i>Liu et al., 2021</i>	PCR primers	CTCAGCCGGTAAATTCCAAA
Sequence-based reagent	Mouse <i>Kcnmb1_F</i>	This paper	PCR primers	ACAACTGTGCTGCCCTCTA
Sequence-based reagent	Mouse <i>Kcnmb1_R</i>	This paper	PCR primers	CACTGTTGGTTTTGATCCCG
Sequence-based reagent	Mouse <i>Kcnmb2_F</i>	This paper	PCR primers	TCAGGAGACACCAACACTTC
Sequence-based reagent	Mouse <i>Kcnmb2_R</i>	This paper	PCR primers	AGTTAGTTTCACCATAGCAA
Sequence-based reagent	Mouse <i>Kcnmb3_F</i>	This paper	PCR primers	GTGGATGACGGGCTGGACTT
Sequence-based reagent	Mouse <i>Kcnmb3_R</i>	This paper	PCR primers	GCACTGGGGTTGGTCTGA
Sequence-based reagent	Mouse <i>Kcnmb4_F</i>	This paper	PCR primers	CTCCTGACCAACCCCAAGT
Sequence-based reagent	Mouse <i>Kcnmb4_R</i>	This paper	PCR primers	TAAAATAGCAAGTGAATGGC
Sequence-based reagent	Mouse <i>Kcnn1_F</i>	<i>Liu et al., 2021</i>	PCR primers	TCAAAAATGCTGCTGCAAAC
Sequence-based reagent	Mouse <i>Kcnn1_R</i>	<i>Liu et al., 2021</i>	PCR primers	TCGTTCACCTTCCCTTGTTT
Sequence-based reagent	Mouse <i>Kcnn2_F</i>	<i>Liu et al., 2021</i>	PCR primers	GATCTGGCAAAGACCCAGAA
Sequence-based reagent	Mouse <i>Kcnn2_R</i>	<i>Liu et al., 2021</i>	PCR primers	GAAGTCCCTTTGCTGCTGTC
Sequence-based reagent	Mouse <i>Kcnn3_F</i>	<i>Liu et al., 2021</i>	PCR primers	ACTTCAACACCCGATTGCTC
Sequence-based reagent	Mouse <i>Kcnn3_R</i>	<i>Liu et al., 2021</i>	PCR primers	GGAAAGGAACGTGATGGAGA
Sequence-based reagent	Mouse <i>Kcnn4_F</i>	<i>Liu et al., 2021</i>	PCR primers	GGCACCTCACAGACACACTG
Sequence-based reagent	Mouse <i>Kcnn4_R</i>	<i>Liu et al., 2021</i>	PCR primers	TTTCTCCGCTTGTGAACT
Sequence-based reagent	Mouse <i>Plcb1_F</i>	<i>Yamazaki et al., 2011</i>	PCR primers	CCCAAGTTGCGTGAAGTCTT
Sequence-based reagent	Mouse <i>Plcb1_R</i>	<i>Yamazaki et al., 2011</i>	PCR primers	GTTGCCAAGCTGAAAACCTC
Sequence-based reagent	Mouse <i>Plcb2_F</i>	<i>Yamazaki et al., 2011</i>	PCR primers	ACATCCAGGAAGTGGTCCAG
Sequence-based reagent	Mouse <i>Plcb2_R</i>	<i>Yamazaki et al., 2011</i>	PCR primers	CGCACCGACTCCTTTACTTC
Sequence-based reagent	Mouse <i>Plcb3_F</i>	<i>Yamazaki et al., 2011</i>	PCR primers	CAGGCCAGCACAGAGACATA
Sequence-based reagent	Mouse <i>Plcb3_R</i>	<i>Yamazaki et al., 2011</i>	PCR primers	AGGATGCTGGCAATCAAATC
Sequence-based reagent	Mouse <i>Plcg1_F</i>	This paper	PCR primers	AACGCTTTGAGGACTGGAGA

Continued on next page

Continued

Reagent type (species) or resource	Designation	Source or reference	Identifiers	Additional information
Sequence-based reagent	Mouse <i>Plcg1</i> _R	This paper	PCR primers	CTCCTCAATCTCTCGCAAGG
Sequence-based reagent	Mouse <i>Plcg2</i> _F	This paper	PCR primers	AACCCCAACCCACACGAGTC
Sequence-based reagent	Mouse <i>Plcg2</i> _R	This paper	PCR primers	AATGTTTCACCTTGCCCTG
Sequence-based reagent	Mouse <i>Trpm7</i> _F	Qian et al., 2019	PCR primers	ATTGCTTAGTTTTGGTGTTC
Sequence-based reagent	Mouse <i>Trpm7</i> _R	Qian et al., 2019	PCR primers	GATTGTGGGAGAGTGGAGT
Sequence-based reagent	Mouse <i>Camk2a</i> _F	This paper	PCR primers	CACCACCATTGAGGACGAAG
Sequence-based reagent	Mouse <i>Camk2a</i> _R	This paper	PCR primers	GGTTCAAAGGCTGTCTATTCC
Sequence-based reagent	Mouse <i>Camk2b</i> _F	This paper	PCR primers	AAGCAGATGGAGTCAAGCC
Sequence-based reagent	Mouse <i>Camk2b</i> _R	This paper	PCR primers	TGCTGTGGGAAGATTCCAGG
Sequence-based reagent	Mouse <i>Camk2d</i> _F	This paper	PCR primers	GATAACAACAAAGCCAACG
Sequence-based reagent	Mouse <i>Camk2d</i> _R	This paper	PCR primers	GTAAGCTCAAAGTCCCAT
Sequence-based reagent	Mouse <i>Camk2g</i> _F	This paper	PCR primers	CAAGAACAGCAAGCCTATCC
Sequence-based reagent	Mouse <i>Camk2g</i> _R	This paper	PCR primers	CCTCTGACTGACTGGTGCGA
Sequence-based reagent	Mouse <i>Pde2a</i> _F	This paper	PCR primers	ATCTTTGACCACTTCTCTCG
Sequence-based reagent	Mouse <i>Pde2a</i> _R	This paper	PCR primers	CATAACCACTTCAGCCATC
Sequence-based reagent	Mouse <i>Pde3a</i> _F	This paper	PCR primers	AACTATACCTGCTCGGACTC
Sequence-based reagent	Mouse <i>Pde3a</i> _R	This paper	PCR primers	TTCGTGCGGCTTTATGCTGG
Sequence-based reagent	Mouse <i>Pde3b</i> _F	This paper	PCR primers	ATTCAAAGCAGAGGTCATC
Sequence-based reagent	Mouse <i>Pde3b</i> _R	This paper	PCR primers	GTTAGAGAGCCAGCAGACAC
Sequence-based reagent	Mouse <i>Pde5a</i> _F	This paper	PCR primers	GACCCTTGCGTTGCTCATTG
Sequence-based reagent	Mouse <i>Pde5a</i> _R	This paper	PCR primers	TGATGGAGTGACAGTACAGC
Sequence-based reagent	Mouse <i>Pde6a</i> _F	This paper	PCR primers	AACCCACCCGCTGACCACTG
Sequence-based reagent	Mouse <i>Pde6a</i> _R	This paper	PCR primers	CTCTTCTTCTTGTGACGA
Sequence-based reagent	Mouse <i>Pde6b</i> _F	This paper	PCR primers	TCCGGGCCTATCTAAACTGC
Sequence-based reagent	Mouse <i>Pde6b</i> _R	This paper	PCR primers	AGAAGACAATTTCCCGGCCAT

Continued on next page

Continued

Reagent type (species) or resource	Designation	Source or reference	Identifiers	Additional information
Sequence-based reagent	Mouse <i>Pde6c</i> _F	This paper	PCR primers	TTGCTCAGGAAATGGTTATG
Sequence-based reagent	Mouse <i>Pde6c</i> _R	This paper	PCR primers	GAAACAGAACTCGTACAGGT
Sequence-based reagent	Mouse <i>Pde6d</i> _F	This paper	PCR primers	CCCAAGAAAATCCTCAAGTG
Sequence-based reagent	Mouse <i>Pde6d</i> _R	This paper	PCR primers	ACAAAGCCAAACTCGAAGAA
Sequence-based reagent	Mouse <i>Pde6g</i> _F	This paper	PCR primers	AAGGGTGAGATTCGGTCAGC
Sequence-based reagent	Mouse <i>Pde6g</i> _R	This paper	PCR primers	TCATCCCCAAACCCTTGAC
Sequence-based reagent	Mouse <i>Pde6h</i> _F	This paper	PCR primers	GGCAGACTCGACAGTTCAAGA
Sequence-based reagent	Mouse <i>Pde6h</i> _R	This paper	PCR primers	CTCCAGATGGCTGAACGCT
Sequence-based reagent	Mouse <i>Pde10a</i> _F	This paper	PCR primers	CATCCGCAAAGCCATCATCG
Sequence-based reagent	Mouse <i>Pde10a</i> _R	This paper	PCR primers	TCTCATCACCTCAGCCCAG
Sequence-based reagent	Mouse <i>Lpar1</i> _F	This paper	PCR primers	GCTTGGTGCCTTTATTGTCT
Sequence-based reagent	Mouse <i>Lpar1</i> _R	This paper	PCR primers	GGTAGGAGTAGATGATGGGG
Sequence-based reagent	Mouse <i>Lpar2</i> _F	This paper	PCR primers	AGTGTGCTGGTATTGCTGAC
Sequence-based reagent	Mouse <i>Lpar2</i> _R	This paper	PCR primers	TTTGATGGAGAGCCTGGCAG
Sequence-based reagent	Mouse <i>Lpar3</i> _F	This paper	PCR primers	ACTTTCCTTCTACTACCTG
Sequence-based reagent	Mouse <i>Lpar3</i> _R	This paper	PCR primers	GTCTTCCACAGCAATAACC
Sequence-based reagent	Mouse <i>Lpar4</i> _F	This paper	PCR primers	CCTCAGTGGTGGTATTTCAG
Sequence-based reagent	Mouse <i>Lpar4</i> _R	This paper	PCR primers	CACAGAAGAACAAGAAACAT
Sequence-based reagent	Mouse <i>Lpar5</i> _F	This paper	PCR primers	AACACGACTTCTACCAACAG
Sequence-based reagent	Mouse <i>Lpar5</i> _R	This paper	PCR primers	AAGACCCAGAGAGCCAGAGC
Sequence-based reagent	Mouse <i>Lpar6</i> _F	This paper	PCR primers	TACTTTGCCATTCGGATTT
Sequence-based reagent	Mouse <i>Lpar6</i> _R	This paper	PCR primers	GCACTTCTCCCATCACTGT
Sequence-based reagent	Mouse <i>Atp2a1</i> _F	Liu et al., 2021	PCR primers	CAAAACAGGGACCCTCACCA
Sequence-based reagent	Mouse <i>Atp2a1</i> _R	Liu et al., 2021	PCR primers	GCCAGTGATGGAGAACTCGT
Sequence-based reagent	Mouse <i>Atp2a2</i> _F	Liu et al., 2021	PCR primers	AAACCAGATGTCCGTGTGCA

Continued on next page

Continued

Reagent type (species) or resource	Designation	Source or reference	Identifiers	Additional information
Sequence-based reagent	Mouse <i>Atp2a2</i> _R	<i>Liu et al., 2021</i>	PCR primers	TGATGGCACTTCACTGGCTT
Sequence-based reagent	Mouse <i>Atp2a3</i> _F	<i>Liu et al., 2021</i>	PCR primers	CCTCGGTCATCTGCTCTGAC
Sequence-based reagent	Mouse <i>Atp2a3</i> _R	<i>Liu et al., 2021</i>	PCR primers	CGTGGTACCCGAAATGGTGA
Sequence-based reagent	Mouse <i>Pln</i> _F	This paper	PCR primers	TACCTCACTCGCTCGGCTAT
Sequence-based reagent	Mouse <i>Pln</i> _R	This paper	PCR primers	TGACGGAGTGCTCGGCTTTA
Sequence-based reagent	Mouse <i>Sox9</i> _F	<i>Qian et al., 2019</i>	PCR primers	AGGAAGCTGGCAGACCAGTA
Sequence-based reagent	Mouse <i>Sox9</i> _R	<i>Qian et al., 2019</i>	PCR primers	CGTTCTTCACCGACTTCCTC
Sequence-based reagent	Mouse <i>Sox5</i> _F	<i>Qian et al., 2019</i>	PCR primers	CTCGTGGAAGCTATGACC
Sequence-based reagent	Mouse <i>Sox5</i> _R	<i>Qian et al., 2019</i>	PCR primers	GATGGGGATCTGTGCTTGTT
Sequence-based reagent	Mouse <i>Sox6</i> _F	<i>Qian et al., 2019</i>	PCR primers	GGATTGGGGAGTACAAGCAA
Sequence-based reagent	Mouse <i>Sox6</i> _R	<i>Qian et al., 2019</i>	PCR primers	CATCTGAGGTGATGGTGTGG
Sequence-based reagent	Mouse <i>Runx2</i> _F	<i>Qian et al., 2019</i>	PCR primers	GCCGGGAATGATGAGAATA
Sequence-based reagent	Mouse <i>Runx2</i> _R	<i>Qian et al., 2019</i>	PCR primers	GGACCGTCCACTGTCACTTT
Sequence-based reagent	Mouse <i>Pthlh</i> _F	<i>Qian et al., 2019</i>	PCR primers	CTCCAACACCAAAAACCAC
Sequence-based reagent	Mouse <i>Pthlh</i> _R	<i>Qian et al., 2019</i>	PCR primers	GCTTGCCTTTCTTCTTCTC
Sequence-based reagent	Mouse <i>Acan</i> _F	<i>Qian et al., 2019</i>	PCR primers	CCTCACCATCCCCTGCTACT
Sequence-based reagent	Mouse <i>Acan</i> _R	<i>Qian et al., 2019</i>	PCR primers	ACTTGATTCTGGGGTGAGG
Sequence-based reagent	Mouse <i>Col10a1</i> _F	<i>Qian et al., 2019</i>	PCR primers	CAAGCCAGGCTATGGAAGTC
Sequence-based reagent	Mouse <i>Col10a1</i> _R	<i>Qian et al., 2019</i>	PCR primers	AGCTGGGCCAATATCTCCTT
Sequence-based reagent	Mouse <i>Col2a1</i> _F	<i>Qian et al., 2019</i>	PCR primers	CACACTGGTAAGTGGGGCAAGACCG
Sequence-based reagent	Mouse <i>Col2a1</i> _R	<i>Qian et al., 2019</i>	PCR primers	GGATTGTGTTGTTTCAGGGTTCGGG
Sequence-based reagent	Mouse <i>18 S</i> _F	<i>Qian et al., 2019</i>	PCR primers	AGACAAATCGCTCCACCAAC
Sequence-based reagent	Mouse <i>18 S</i> _R	<i>Qian et al., 2019</i>	PCR primers	CTCAACACGGGAAACCTCAC
Sequence-based reagent	Mouse <i>Actb</i> _F	<i>Qian et al., 2019</i>	PCR primers	CATCCGTAAAGACCTCTATGCCAAC
Sequence-based reagent	Mouse <i>Actb</i> _R	<i>Qian et al., 2019</i>	PCR primers	ATGGAGCCACCGATCCACA

Continued on next page

Continued

Reagent type (species) or resource	Designation	Source or reference	Identifiers	Additional information
Sequence-based reagent	Mouse <i>Gapdh</i> _F	Qian et al., 2019	PCR primers	TGTGTCCGTCGTGGATCTGA
Sequence-based reagent	Mouse <i>Gapdh</i> _R	Qian et al., 2019	PCR primers	TTGCTGTTGAAGTCGCAGGAG
Peptide, recombinant protein	ANP (Human, 1–28)	Peptide Institute	Cat#4135	
Peptide, recombinant protein	CNP-22 (Human)	Peptide Institute	Cat#4229	
Commercial assay or kit	Amersham ECL Prime Western Blotting Detection Reagent	Cytiva	Cat#RPN2232	
Commercial assay or kit	ISOGEN	NipponGene	Cat#319-90211	
Commercial assay or kit	ReverTra Ace qPCR RT Master Mix with gDNA Remover	TOYOBO	Cat#FSQ-301	
Chemical compound, drug	FTY720	Sigma-Aldrich	SML0700; CAS: 162359-56-0	
Chemical compound, drug	Fura-2 AM	DOJINDO	F025; CAS: 108964-32-5	
Chemical compound, drug	Hyaluronidase from sheep testes	Sigma-Aldrich	H2126; CAS: 37326-33-3	
Chemical compound, drug	KN93	WAKO	115-00641; CAS: 139298-40-1	
Chemical compound, drug	KT5823	Cayman Chemical	10010965; CAS: 126643-37-6	
Chemical compound, drug	NNC 550396 dihydrochloride	Tocris Bioscience	2268; CAS: 357400-13-6	
Chemical compound, drug	NS1619	Sigma-Aldrich	N170; CAS: 153587-01-0	
Chemical compound, drug	1-Oleoyl lysophosphatidic acid	Cayman Chemical	62215; CAS: 325465-93-8	
Chemical compound, drug	Oxonol VI	Sigma-Aldrich	75926; CAS: 64724-75-0	
Chemical compound, drug	Paxilline	Tocris Bioscience	2006; CAS: 57186-25-1	
Chemical compound, drug	8-pCPT-cGMP	Biolog	C009; CAS: 51239-26-0	
Chemical compound, drug	Thapsigargin	Nacalai Tesque	33637-31; CAS: 67526-95-8	
Chemical compound, drug	U73122	Sigma-Aldrich	U6756; CAS: 112648-68-7	
Software, algorithm	Adobe Illustrator	Adobe Systems	http://www.adobe.com/products/illustrator.html	
Software, algorithm	GraphPad Prism v7	GraphPad	https://www.graphpad.com/	
Software, algorithm	ImageJ	N/A	https://imagej.nih.gov/ij/	
Software, algorithm	Leica Application Suite X	Leica Microsystems	https://www.leica-microsystems.com/products/microscope-software/p/leica-las-x-ls/	

Reagents, primers, and mice

Reagents and antibodies used in this study, and synthetic primers used for RT-PCR analysis and mouse genotyping are listed in Key Resources Table. C57BL mice were used as wild-type mice in this study. Chondrocyte-specific *Trpm7*-knockout mice with C57BL genetic background were generated by crossing *Trpm7*^{fl/fl} mice (**Qian et al., 2019**) with transgenic mice carrying *Col11a2-Cre*, originally

designated as *11Enh-Cre* (Iwai et al., 2008) Using primer sets for detecting *Col11a2-Cre* transgene and *Trpm7* alleles, we previously reported that *Trpm7* is specifically inactivated in cartilage tissues from the *Trpm7^{fl}*, *Col11a2-Cre^{+/-}* mice (Qian et al., 2019). Chondrocyte-specific *Npr2*-knockout mice with C57BL background were generated as previously described (Nakao et al., 2015), and we designed primers for detecting the *Col2a1-Cre* transgene and the floxed *Npr2* gene in this study (Figure 1—figure supplement 1).

Bone slice preparations

Femoral bones were isolated from E17.5 mice and immersed in a physiological salt solution (PSS): (in mM) 150 NaCl, 4 KCl, 1 MgCl₂, 2 CaCl₂, 5.6 glucose, and 5 2-[4-(2-Hydroxyethyl)-1-piperazinyl]ethanesulfonic acid (HEPES, pH 7.4). Longitudinal bone slices (~40 μm thickness) were prepared using a vibrating microslicer (DTK-1000N, Dosaka EM Co., Japan) as previously described (Qian et al., 2019).

Ca²⁺ imaging

Fura-2 Ca²⁺ imaging of bone slices was performed as previously described (Qian et al., 2019). Briefly, bone slices placed on glass-bottom dishes (Matsunami, Japan) were incubated in PSS containing 15 μM Fura-2AM for 1 hr at 37°C. Fluorescence microscopy distinguished round, columnar, and hypertrophic chondrocytes with characteristic morphological features in the bone slices loaded with Fura-2. For ratiometric imaging, excitation light of 340 and 380 nm was alternately delivered, and emission light of >510 nm was detected by a cooled EM-CCD camera (Model C9100-13; Hamamatsu Photonics, Japan) mounted on an upright fluorescence microscope (DM6 FS, Leica) using a ×40 water-immersion objective (HCX APO L, Leica). In typical measurements, ~30 round chondrocytes were randomly examined in each slice preparation to select the Ca²⁺ fluctuation-positive cells generating spontaneous events (>0.025 in Fura-2 ratio) using commercial software (Leica Application Suite X), and recording traces from the positive cells were then analyzed using Fiji/ImageJ software (US. NIH) for examining Ca²⁺ fluctuation amplitude and frequency. Imaging experiments were performed at room temperature (23–25°C) and PSS was used as the normal bathing solution. For the pretreatments of CNP, ANP, and 8-pCPT-cGMP, bone slices were immersed in PSS with the indicated compound for 1 hr at room temperature after Fura-2 loading.

Membrane potential monitoring

Bone slices were perfused with the PSS containing 200 nM oxonol VI at room temperature and analyzed as previously described (Yamazaki et al., 2011). To prepare the calibration plot showing the relationship between the fluorescence intensity and membrane potential, saline solutions containing 20, 40, 60, or 100 mM KCl were used as bathing solutions. Fluorescence images with excitation at 559 nm and emission at >606 nm were captured at a sampling rate of ~7.0 s using a confocal laser scanning microscope (FV1000; Olympus).

Immunochemical analysis of CaMKII

Bone slices were pretreated with or without CNP were subjected to immunochemical assessments as previously described (Li et al., 2011). Briefly, for immunohistochemical analysis, bone slices were fixed in 4% paraformaldehyde and treated with 1% hyaluronidase to enhance immunodetection (Ahrens and Dudley, 2011; Mouser et al., 2016). After blocking with fetal bovine serum-containing solution, bone slices were reacted with primary and Alexa 488-conjugated secondary antibodies and observed with a confocal microscope (FV1000; Olympus). For immunoblot analysis, bone slices were lysed in the buffer containing 4% sodium dodecyl sulfate, 20 mM Tris-HCl (pH 8.8) and a phosphatase inhibitor cocktail (100 mM NaF, 10 mM Na₃PO₄, 1 mM Na₂VO₃, and 20 mM β-glycerophosphate). The resulting lysate proteins were electrophoresed on sodium dodecyl sulfate-polyacrylamide gels and electroblotted onto nylon membranes for immunodetection using primary and Horseradish peroxidase (HRP)-conjugated secondary antibodies. Antigen proteins were visualized using a chemiluminescence reagent and image analyzer (Amersham Imager 600, Cytiva). The immunoreactivities yielded were quantitatively analyzed by means of Fiji/ImageJ software.

Metatarsal organ culture

Metatarsal bone rudiments were cultured as previously described (*Houston et al., 2016*). Briefly, the three central metatarsal rudiments were dissected from E15.5 mice and cultured in α MEM containing 5 μ g/ml ascorbic acid, 1 mM β -glycerophosphate pentahydrate, 100 units/ml penicillin, 100 μ g/ml streptomycin and 0.2% bovine serum albumin (fatty acid free). The explants were analyzed under a photomicroscope (BZ-X710, Keyence, Japan) for size measurements using Fiji/ImageJ software.

Histological analysis

For histological analysis, cultured bones were fixed in 4% paraformaldehyde, embedded in Super Cryoembedding Medium (Section-lab, Japan), and frozen in liquid nitrogen. Serial cryosections (6 μ m in thickness) were prepared from the fixed specimens and stained with hematoxylin and eosin. In the sectional images, round, columnar, and hypertrophic chondrocytes were distinguished by their characteristic morphological features. Microscopic images were quantitatively analyzed using Fiji/ImageJ software.

Gene expression analysis

Quantitative RT-PCR analysis was performed as previously described (*Zhao et al., 2016*). From femoral epiphyses, the terminal region containing round chondrocytes and the adjacent region enriched with columnar and hypertrophic chondrocytes were separated under stereo-microscope. Femoral and humeral specimens were subjected to total RNA preparation using a commercial reagent (Isogen) for cDNA synthesis using a commercial kit (ReverTra ACE qPCR-RT kit). The resulting cDNAs were examined by real-time PCR (LightCycler 480 II, Roche), and the cycle threshold was determined from the amplification curve as an index for relative mRNA content in each reaction.

Quantification and statistical analysis

All data obtained are presented as the means \pm standard error of the mean with n values indicating the number of examined mice. Student t -test and analysis of variance were used for two-group and multiple group comparisons, respectively (Prism 7, GraphPad Software Inc): $p < 0.05$ was considered to be statistically significant.

Acknowledgements

We thank Jun Matsushita (Graduate School of Pharmaceutical Sciences, Kyoto University) for mouse in vitro fertilization. This work was supported in part by the MEXT/JSPS (KAKENHI Grant Number 21H02663, 20H03802, and 21K19565), Platform Project for Supporting Drug Discovery and Life Science Research (JP19am0101092j0003), Takeda Science Foundation, Kobayashi International Scholarship Foundation, the NAKATOMI Foundation, Vehicle Racing Commemorative Foundation, The Mother and Child Health Foundation, and Japan Foundation for Applied Enzymology. Y.M. is grateful for Fujita Jinsei Scholarship from Graduate School of Pharmaceutical Sciences, Kyoto University. F.L. is grateful for Scholarship from Graduate Program for Medical Innovation, Kyoto University, and Otsuka Toshimi Scholarship Foundation.

Additional information

Funding

Funder	Grant reference number	Author
Japan Society for the Promotion of Science	21H02663	Hiroshi Takeshima
Japan Society for the Promotion of Science	20H03802	Atsuhiko Ichimura
Japan Society for the Promotion of Science	21K19565	Atsuhiko Ichimura

Funder	Grant reference number	Author
Japan Agency for Medical Research and Development	JP19am0101092j0003	Hiroshi Takeshima
Takeda Medical Research Foundation		Atsuhiko Ichimura
Kobayashi International Scholarship Foundation		Atsuhiko Ichimura
Nakatomi Foundation		Atsuhiko Ichimura
Vehicle Racing Commemorative Foundation		Hiroshi Takeshima
Mother and Child Health Foundation		Atsuhiko Ichimura

The funders had no role in study design, data collection, and interpretation, or the decision to submit the work for publication.

Author contributions

Yuu Miyazaki, Data curation, Formal analysis, Investigation, Methodology, Validation, Visualization, Writing – original draft, Writing – review and editing; Atsuhiko Ichimura, Conceptualization, Data curation, Formal analysis, Funding acquisition, Investigation, Project administration, Resources, Validation, Visualization, Writing – original draft, Writing – review and editing; Ryo Kitayama, Naoki Okamoto, Tomoki Yasue, Feng Liu, Takaaki Kawabe, Hiroki Nagatomo, Data curation, Investigation, Methodology; Yohei Ueda, Data curation, Funding acquisition, Investigation, Methodology, Resources; Ichiro Yamauchi, Conceptualization, Data curation, Investigation, Resources; Takuro Hakata, Kazumasa Nakao, Investigation, Resources; Sho Kakizawa, Data curation, Investigation; Miyuki Nishi, Data curation, Investigation, Validation; Yasuo Mori, Haruhiko Akiyama, Resources, Validation; Kazuwa Nakao, Conceptualization, Resources, Validation; Hiroshi Takeshima, Conceptualization, Data curation, Funding acquisition, Investigation, Project administration, Resources, Supervision, Validation, Visualization, Writing – original draft, Writing – review and editing

Author ORCIDs

Atsuhiko Ichimura  <http://orcid.org/0000-0003-0366-5211>
Hiroshi Takeshima  <http://orcid.org/0000-0003-4525-3725>

Ethics

All experiments in this study were conducted with the approval of the Animal Research Committee according to the regulations on animal experimentation at Kyoto University.

Decision letter and Author response

Decision letter <https://doi.org/10.7554/eLife.71931.sa1>

Author response <https://doi.org/10.7554/eLife.71931.sa2>

Additional files

Supplementary files

- Transparent reporting form

Data availability

All data generated or analysed during this study are included in the manuscript and supporting files. Source data files have been provided for Figures 1, 2, 3, 4, 5, 6, 7 and 8.

References

- Ahrens MJ, Dudley AT. 2011. Chemical pretreatment of growth plate cartilage increases immunofluorescence sensitivity. *The Journal of Histochemistry and Cytochemistry* **59**:408–418. DOI: <https://doi.org/10.1369/0022155411400869>, PMID: 21411811

- Berendsen AD**, Olsen BR. 2015. Bone development. *Bone* **80**:14–18. DOI: <https://doi.org/10.1016/j.bone.2015.04.035>, PMID: 26453494
- Bibli S-I**, Andreadou I, Chatzianastasiou A, Tzimas C, Sanoudou D, Kranias E, Brouckaert P, Coletta C, Szabo C, Kremastinos DT, Iliodromitis EK, Papapetropoulos A. 2015. Cardioprotection by H₂S engages a cGMP-dependent protein kinase G/phospholamban pathway. *Cardiovascular Research* **106**:432–442. DOI: <https://doi.org/10.1093/cvr/cvv129>, PMID: 25870184
- Clark RB**, Hatano N, Kondo C, Belke DD, Brown BS, Kumar S, Votta BJ, Giles WR. 2010. Voltage-gated K⁺ currents in mouse articular chondrocytes regulate membrane potential. *Channels (Austin, Tex.)* **4**:179–191. DOI: <https://doi.org/10.4161/chan.4.3.11629>, PMID: 20372061
- Dong D-L**, Yue P, Yang B-F, Wang W-H. 2008. Hydrogen peroxide stimulates the Ca²⁺-activated big-conductance K channels (BK) through cGMP signaling pathway in cultured human endothelial cells. *Cellular Physiology and Biochemistry* **22**:119–126. DOI: <https://doi.org/10.1159/000149789>, PMID: 18769038
- Fleig A**, Chubanov V. 2014. TRPM7. Fleig A (Ed). *Handbook of Experimental Pharmacology*. Springer. p. 521–546. DOI: https://doi.org/10.1007/978-3-642-54215-2_21, PMID: 24756720
- Fukao M**, Mason HS, Britton FC, Kenyon JL, Horowitz B, Keef KD. 1999. Cyclic GMP-dependent protein kinase activates cloned BKCa channels expressed in mammalian cells by direct phosphorylation at serine 1072. *The Journal of Biological Chemistry* **274**:10927–10935. DOI: <https://doi.org/10.1074/jbc.274.16.10927>, PMID: 10196172
- Guo JY**, Zhang MH, Jiang JZ, Piao LH, Fang XS, Jin Z, Cai YL. 2018. The role of CNP-mediated PKG/PKA-PLC β pathway in diabetes-induced gastric motility disorder. *Peptides* **110**:47–55. DOI: <https://doi.org/10.1016/j.peptides.2018.10.012>, PMID: 30391424
- Houston DA**, Staines KA, MacRae VE, Farquharson C. 2016. Culture of Murine Embryonic Metatarsals: A Physiological Model of Endochondral Ossification. *Journal of Visualized Experiments* **1**:e54978. DOI: <https://doi.org/10.3791/54978>, PMID: 28060328
- Huang J**, Zhou H, Mahavadi S, Sriwai W, Murthy KS. 2007. Inhibition of Galphaq-dependent PLC-beta1 activity by PKG and PKA is mediated by phosphorylation of RGS4 and GRK2. *American Journal of Physiology. Cell Physiology* **292**:C200–C208. DOI: <https://doi.org/10.1152/ajpcell.00103.2006>, PMID: 16885398
- Iwai T**, Murai J, Yoshikawa H, Tsumaki N. 2008. Smad7 inhibits chondrocyte differentiation at multiple steps during endochondral bone formation and down-regulates p38 MAPK pathways. *The Journal of Biological Chemistry* **283**:27154–27164. DOI: <https://doi.org/10.1074/jbc.M801175200>, PMID: 18644788
- Kawasaki Y**, Kugimiya F, Chikuda H, Kamekura S, Ikeda T, Kawamura N, Saito T, Shinoda Y, Higashikawa A, Yano F, Ogasawara T, Ogata N, Hoshi K, Hofmann F, Woodgett JR, Nakamura K, Chung U, Kawaguchi H. 2008. Phosphorylation of GSK-3 β by cGMP-dependent protein kinase II promotes hypertrophic differentiation of murine chondrocytes. *The Journal of Clinical Investigation* **118**:2506–2515. DOI: <https://doi.org/10.1172/JCI35243>, PMID: 18551195
- Krejci P**, Masri B, Fontaine V, Mekikian PB, Weis M, Prats H, Wilcox WR. 2005. Interaction of fibroblast growth factor and C-natriuretic peptide signaling in regulation of chondrocyte proliferation and extracellular matrix homeostasis. *Journal of Cell Science* **118**:5089–5100. DOI: <https://doi.org/10.1242/jcs.02618>, PMID: 16234329
- Kubacka M**, Kotańska M, Kazek G, Waszkielewicz AM, Marona H, Filippek B, Mogilski S. 2018. Involvement of the NO/sGC/cGMP/K⁺ channels pathway in vascular relaxation evoked by two non-quinazoline α_1 -adrenoceptor antagonists. *Biomedicine & Pharmacotherapy = Biomedicine & Pharmacotherapie* **103**:157–166. DOI: <https://doi.org/10.1016/j.biopha.2018.04.034>, PMID: 29653360
- Lalli MJ**, Shimizu S, Sutliff RL, Kranias EG, Paul RJ. 1999. [Ca²⁺]_i homeostasis and cyclic nucleotide relaxation in aorta of phospholamban-deficient mice. *The American Journal of Physiology* **277**:H963–H970. DOI: <https://doi.org/10.1152/ajpheart.1999.277.3.H963>, PMID: 10484417
- Li Y**, Ahrens MJ, Wu A, Liu J, Dudley AT. 2011. Calcium/calmodulin-dependent protein kinase II activity regulates the proliferative potential of growth plate chondrocytes. *Development (Cambridge, England)* **138**:359–370. DOI: <https://doi.org/10.1242/dev.052324>, PMID: 21177348
- Liang L**, Li X, Moutton S, Schrier Vergano SA, Cogné B, Saint-Martin A, Hurst ACE, Hu Y, Bodamer O, Thevenon J, Hung CY, Isidor B, Gerard B, Rega A, Nambot S, Lehalle D, Duffourd Y, Thauvin-Robinet C, Faivre L, Bézieau S, et al. 2019. De novo loss-of-function KCNMA1 variants are associated with a new multiple malformation syndrome and a broad spectrum of developmental and neurological phenotypes. *Human Molecular Genetics* **28**:2937–2951. DOI: <https://doi.org/10.1093/hmg/ddz117>, PMID: 31152168
- Liu F**, Xu L, Nishi M, Ichimura A, Takeshima H. 2021. Enhanced Ca²⁺ handling in thioglycolate-elicited peritoneal macrophages. *Cell Calcium* **96**:102381. DOI: <https://doi.org/10.1016/j.ceca.2021.102381>, PMID: 33647639
- Martel G**, Hamet P, Tremblay J. 2010. Central role of guanylyl cyclase in natriuretic peptide signaling in hypertension and metabolic syndrome. *Molecular and Cellular Biochemistry* **334**:53–65. DOI: <https://doi.org/10.1007/s11010-009-0326-8>, PMID: 19937369
- Miyazawa T**, Ogawa Y, Chusho H, Yasoda A, Tamura N, Komatsu Y, Pfeifer A, Hofmann F, Nakao K. 2002. Cyclic GMP-dependent protein kinase II plays a critical role in C-type natriuretic peptide-mediated endochondral ossification. *Endocrinology* **143**:3604–3610. DOI: <https://doi.org/10.1210/en.2002-220307>, PMID: 12193576
- Mouser VHM**, Melchels FPW, Visser J, Dhert WJA, Gawlitta D, Malda J. 2016. Yield stress determines bioprintability of hydrogels based on gelatin-methacryloyl and gellan gum for cartilage bioprinting. *Biofabrication* **8**:035003. DOI: <https://doi.org/10.1088/1758-5090/8/3/035003>, PMID: 27431733
- Nakao K**, Itoh H, Saito Y, Mukoyama M, Ogawa Y. 1996. The natriuretic peptide family Curr Opin Nephrol Hypertens. *Current Opinion in Nephrology and Hypertension* **5**:4–11. DOI: <https://doi.org/10.1097/00041552-199601000-00003>

- Nakao K**, Osawa K, Yasoda A, Yamanaka S, Fujii T, Kondo E, Koyama N, Kanamoto N, Miura M, Kuwahara K, Akiyama H, Bessho K, Nakao K. 2015. The Local CNP/GC-B system in growth plate is responsible for physiological endochondral bone growth. *Scientific Reports* **5**:10554. DOI: <https://doi.org/10.1038/srep10554>, PMID: 26014585
- Nalli AD**, Kumar DP, Al-Shboul O, Mahavadi S, Kuemmerle JF, Grider JR, Murthy KS. 2014. Regulation of G β γ -dependent PLC- β 3 activity in smooth muscle: inhibitory phosphorylation of PLC- β 3 by PKA and PKG and stimulatory phosphorylation of G α i-GTPase-activating protein RGS2 by PKG. *Cell Biochemistry and Biophysics* **70**:867–880. DOI: <https://doi.org/10.1007/s12013-014-9992-6>, PMID: 24777815
- Peake NJ**, Hobbs AJ, Pinguan-Murphy B, Salter DM, Berenbaum F, Chowdhury TT. 2014. Role of C-type natriuretic peptide signalling in maintaining cartilage and bone function. *Osteoarthritis and Cartilage* **22**:1800–1807. DOI: <https://doi.org/10.1016/j.joca.2014.07.018>, PMID: 25086404
- Qian N**, Ichimura A, Takei D, Sakaguchi R, Kitani A, Nagaoka R, Tomizawa M, Miyazaki Y, Miyachi H, Numata T, Kakizawa S, Nishi M, Mori Y, Takeshima H. 2019. TRPM7 channels mediate spontaneous Ca²⁺ fluctuations in growth plate chondrocytes that promote bone development. *Science Signaling* **12**:eaaw4847. DOI: <https://doi.org/10.1126/scisignal.aaw4847>, PMID: 30967513
- Raeymaekers L**, Hofmann F, Casteels R. 1988. Cyclic GMP-dependent protein kinase phosphorylates phospholamban in isolated sarcoplasmic reticulum from cardiac and smooth muscle. *The Biochemical Journal* **252**:269–273. DOI: <https://doi.org/10.1042/bj2520269>, PMID: 2844148
- Savarirayan R**, Tofts L, Irving M, Wilcox W, Bacino CA, Hoover-Fong J, Ulloa Font R, Harmatz P, Rutsch F, Bober MB, Polgreen LE, Ginebreda I, Mohnike K, Charrow J, Hoernschemeyer D, Ozono K, Alanay Y, Arundel P, Kagami S, Yasui N, et al. 2020. Once-daily, subcutaneous vosoritide therapy in children with achondroplasia: a randomised, double-blind, phase 3, placebo-controlled, multicentre trial. *Lancet (London, England)* **396**:684–692. DOI: [https://doi.org/10.1016/S0140-6736\(20\)31541-5](https://doi.org/10.1016/S0140-6736(20)31541-5), PMID: 32891212
- Ueda Y**, Yasoda A, Yamashita Y, Kanai Y, Hirota K, Yamauchi I, Kondo E, Sakane Y, Yamanaka S, Nakao K, Fujii T, Inagaki N. 2016. C-type natriuretic peptide restores impaired skeletal growth in a murine model of glucocorticoid-induced growth retardation. *Bone* **92**:157–167. DOI: <https://doi.org/10.1016/j.bone.2016.08.026>, PMID: 27594049
- Vasques GA**, Arnhold IJP, Jorge AAL. 2014. Role of the natriuretic peptide system in normal growth and growth disorders. *Hormone Research in Paediatrics* **82**:222–229. DOI: <https://doi.org/10.1159/000365049>, PMID: 25196103
- White RE**, Kryman JP, El-Mowafy AM, Han G, Carrier GO. 2000. cAMP-dependent vasodilators cross-activate the cGMP-dependent protein kinase to stimulate BK(Ca) channel activity in coronary artery smooth muscle cells. *Circulation Research* **86**:897–905. DOI: <https://doi.org/10.1161/01.res.86.8.897>, PMID: 10785513
- Wit JM**, Camacho-Hübner C. 2011. Endocrine regulation of longitudinal bone growth. *Endocrine Development* **21**:30–41. DOI: <https://doi.org/10.1159/000328119>, PMID: 21865752
- Wit JM**, Oostdijk W, Losekoot M, van Duyvenvoorde HA, Ruivenkamp CAL, Kant SG. 2016. MECHANISMS IN ENDOCRINOLOGY: Novel genetic causes of short stature. *European Journal of Endocrinology* **174**:R145–R173. DOI: <https://doi.org/10.1530/EJE-15-0937>, PMID: 26578640
- Xia C**, Bao Z, Yue C, Sanborn BM, Liu M. 2001. Phosphorylation and regulation of G-protein-activated phospholipase C-beta 3 by cGMP-dependent protein kinases. *The Journal of Biological Chemistry* **276**:19770–19777. DOI: <https://doi.org/10.1074/jbc.M006266200>, PMID: 11278298
- Yamashita T**, Fujii T, Yamauchi I, Ueda Y, Hirota K, Kanai Y, Yasoda A, Inagaki N. 2020. C-Type Natriuretic Peptide Restores Growth Impairment Under Enzyme Replacement in Mice With Mucopolysaccharidosis VII. *Endocrinology* **161**:bqaa008. DOI: <https://doi.org/10.1210/endo/bqaa008>, PMID: 31974587
- Yamazaki D**, Tabara Y, Kita S, Hanada H, Komazaki S, Naitou D, Mishima A, Nishi M, Yamamura H, Yamamoto S, Kakizawa S, Miyachi H, Yamamoto S, Miyata T, Kawano Y, Kamide K, Ogihara T, Hata A, Umemura S, Soma M, et al. 2011. TRIC-A channels in vascular smooth muscle contribute to blood pressure maintenance. *Cell Metabolism* **14**:231–241. DOI: <https://doi.org/10.1016/j.cmet.2011.05.011>, PMID: 21803293
- Yasoda A.**, Ogawa Y, Suda M, Tamura N, Mori K, Sakuma Y, Chusho H, Shiota K, Tanaka K, Nakao K. 1998. Natriuretic Peptide Regulation of Endochondral Ossification. *Journal of Biological Chemistry* **273**:11695–11700. DOI: <https://doi.org/10.1074/jbc.273.19.11695>, PMID: 9565590
- Yasoda A**, Komatsu Y, Chusho H, Miyazawa T, Ozasa A, Miura M, Kurihara T, Rogi T, Tanaka S, Suda M, Tamura N, Ogawa Y, Nakao K. 2004. Overexpression of CNP in chondrocytes rescues achondroplasia through a MAPK-dependent pathway. *Nature Medicine* **10**:80–86. DOI: <https://doi.org/10.1038/nm971>, PMID: 14702637
- Zhao C**, Ichimura A, Qian N, Iida T, Yamazaki D, Noma N, Asagiri M, Yamamoto K, Komazaki S, Sato C, Aoyama F, Sawaguchi A, Kakizawa S, Nishi M, Takeshima H. 2016. Mice lacking the intracellular cation channel TRIC-B have compromised collagen production and impaired bone mineralization. *Science Signaling* **9**:ra49. DOI: <https://doi.org/10.1126/scisignal.aad9055>, PMID: 27188440
- Zois NE**, Bartels ED, Hunter I, Kousholt BS, Olsen LH, Goetze JP. 2014. Natriuretic peptides in cardiometabolic regulation and disease. *Nature Reviews. Cardiology* **11**:403–412. DOI: <https://doi.org/10.1038/nrcardio.2014.64>, PMID: 24820868